267 920

ARF 2152-18
(Final Report)

ARF

ARMOUR RESEARCH FOUNDATION OF ILLINOIS INSTITUTE OF TECHNOLOGY

TECHNOLOGY CENTER

A MECHANISM FOR STRESS-CORROSION EMBRITTLEMENT

Office of Naval Research
Washington 25, D. C.

Contract No. Ncnr-2602(00)

25 years of research
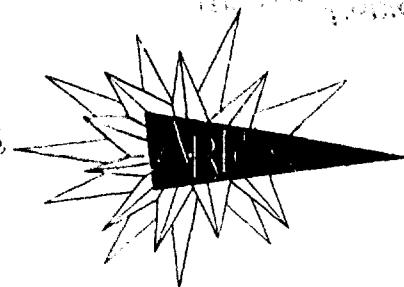
Armour Research Foundation
of
Illinois Institute of Technology
Technology Center
Chicago 16, Illinois

Project No. ARF 2152
Contract No. Nonr-2602(00)

A MECHANISM FOR STRESS-CORROSION EMBRITTLEMENT

Report No. ARF 2152-18
(Final Report)

June 15, 1958 - September 30, 1961

for

Office of Naval Research
Department of the Navy
Washington 25, D. C.

November 27, 1961

ABSTRACT

The stress-corrosion cracking behavior of 304 stainless steel in MgCl$_2$ at 140°C has been studied. Tensile deformation behavior in the vicinity of the yield point suggested that there is no measurable Rebinder Effect or Roscoe Effect. In static tensile tests, the time to failure was found to decrease with applied stress in agreement with previous work. No incubation period prior to the onset of cracking was noted, while varying the time in solution prior to the application of stress had no effect on subsequent stress-induced failure. Prestressing at various temperatures in air in the range 140°-500°C was found to influence subsequent time to failure at 140°C in MgCl$_2$. Cyclic loading treatments were found to have no influence on time to failure, and there was no evidence of rapid crack propagation characteristic of brittle fracture. Prior deformation carried out at various temperatures reduced the susceptibility of 304 stainless steel. Microstructure was also found to strongly influence cracking behavior; strain-induced martensite resulted in a marked increase in resistance to failure.

In the earlier part of the program it was shown through the Stroh-Petch equation relating fracture stress and grain size that stress-corrosion environments can lead to a lowering of the surface energy associated with the formation of fracture surfaces. A variety of materials and corrosion media were examined.

ARMOUR RESEARCH FOUNDATION OF ILLINOIS INSTITUTE OF TECHNOLOGY

ARF 2152-18
(Final Report)

During the final year's work it was demonstrated that the mechanism of stress-corrosion cracking depended on the simultaneous action of both electrochemical and mechanical processes. Using a variety of experimental conditions, efforts to separate the electrochemical and mechanical contributions to the phenomenon proved unsuccessful.

TABLE OF CONTENTS

LIST OF TABLES

ARMOUR RESEARCH FOUNDATION OF ILLINOIS INSTITUTE OF TECHNOLOGY

ARF 2152-18
(Final Report)

LIST OF ILLUSTRATIONS

ARF 2152-18
(Final Report)

LIST OF ILLUSTRATIONS

(Continued)

ARF 2152-18
(Final Report)

LIST OF ILLUSTRATIONS

(Continued)

A MECHANISM FOR STRESS-CORROSION EMBRITTLEMENT

I. SUMMARY

A study of the stress-corrosion cracking behavior of 304 stainless steel in $MgCl_2$ at 140°C has been made which included an examination of the influence of metallurgical and mechanical variables on the phenomenon.

Tensile deformation behavior in the vicinity of the yield point has suggested that there is no measurable Rebinder Effect or Roscoe Effect in fully softened polycrystalline 304 stainless steel. This observation is of importance since it may influence existing theories concerning the roles of surface energy and surface oxide layers on stress-corrosion cracking. In static tensile tests, increasing applied stress decreased the time to failure and increased the crack density. Extension measurements of specimens under test were shown to directly reflect the rate of crack growth.

The incubation period associated with a pre-cracking stage noted by previous investigations was not observed, while varying the time in solution prior to the application of stress had no effect on the subsequent stress-induced failure. These findings throw doubt on the supposed role of an oxide or passive film in determining time to failure by stress-corrosion cracking.

Prestressing of specimens at various temperatures within the range 140°-500°C in air at 50,000 psi prior to testing in $MgCl_2$ at 140°C indicated that the influence of prestressing temperature on time to failure was entirely a strain effect. The greater the prestrain, the longer the time to failure.

ARMOUR RESEARCH FOUNDATION OF ILLINOIS INSTITUTE OF TECHNOLOGY

ARF 2152-18
(Final Report)

Various cyclic loading treatments were found to have no influence on the time to failure of 304 stainless steel. The integrated time at stress remained approximately constant. Also, there was no evidence of rapid crack propagation characteristic of brittle fracture. It was concluded that stress-corrosion cracks propagated slowly and were the result of the simultaneous co-operative action of mechanical and electrochemical phenomena.

Prior deformation at 300° C resulted in a marked increase in time to failure and reduction in the density of surface cracks generated on subsequent testing.

Microstructure was shown to have a strong influence on stress-corrosion cracking behavior. Duplex austenite-carbide structures were found to be less susceptible than single-phase fully softened austenite, while specimens containing strain-induced martensite were the most resistant of all the materials tested.

The Appendix contains a summary of the work carried out during the first two years of the contract. Using the Stroh-Petch equation relating fracture strength and surface energy, the results obtained for a series of alloys suggested that stress-corrosion cracking could be accounted for, in part at least, by a lowering of the surface energy associated with the initiation of fracture surfaces. During these dynamic loading-unloading tests, cracks were observed to initiate but did not grow in a typical brittle fashion, suggesting that a time dependency was involved in cracking.

ARMOUR RESEARCH FOUNDATION OF ILLINOIS INSTITUTE OF TECHNOLOGY

- 2 -   ARF 2152-18
                                         (Final Report)

The interplay between time and stress on crack propagation during stress-corrosion cracking and the possible implications of surface energy formed the basis of the third year's work.

II. INTRODUCTION

This is a final report on Contract No. Nonr-2602(00) describing the work done during the period June 15, 1958, to September 30, 1961. The report includes a detailed account of the results obtained during the past twelve months, together with a summary of the salient features of the first and second years' work. This document, therefore, contains the objectives and achievements of the entire program. However, a comprehensive account of the first two phases of the project is given in reports ARF 2152-7 and ARF 2152-13.

The over-all program had two main objectives:

(1) Analyze the specific behavior characteristics of stress-corrosion embrittlement with the hope that this phenomenon could be brought within the present concepts of brittle fracture.

(2) Study the kinetics of crack growth and the influence of metallurgical and mechanical variables on the stress-corrosion embrittlement phenomenon.

The first two years of the program were devoted to objective (1), and these results are summarized in the Appendix. The second objective was pursued during the final twelve months and is described in detail below.

ARF 2152-18
(Final Report)

III. PREVIOUS WORK

This review of previous work outlines the general characteristics of the stress-corrosion cracking phenomenon in the light of currently accepted concepts of fracture in cyrstalline solids. Emphasis is placed on those features which are thought to be basic to the mechanisms involved and, furthermore, particular attention has been focused on the behavior of austenitic stainless steels since this material was used throughout the last stage of the experimental work.

It is apparent from the large mass of empirical data that has been collected on the phenomenon that two processes exist which are both necessary and sufficient to cause stress-corrosion cracking:

(1) Electrochemical processes

(2) Mechanical processes

The nucleation and growth of cracks is considered to be due to the co-operative action of these two processes. The phenomenological aspects of these processes are now considered, and the contribution they make to our understanding of the mechanism of stress-corrosion cracking is discussed.

A. Electrochemical Processes

A number of investigators[1,2,3] have studied the electrochemical behavior of metals in both the unstressed and the stressed condition when immersed in aqueous solutions known to produce stress-corrosion cracking. The changes in electrode potential of 18-8 stainless steel with time follow the general trend shown in Figure 1; these curves are interpreted as follows.

ARMOUR RESEARCH FOUNDATION OF ILLINOIS INSTITUTE OF TECHNOLOGY

ARF 2152-18
(Final Report)

The initial reduction is caused by the beginning of anodic action at points of imperfection while the rise is due to the partial covering of exposed areas of solid corrosion products. As this process continues, the cathodic areas on the surface expand at the expense of the anodic areas and this is accompanied by a continued rise in potential. In stressed specimens the decrease after the maximum is associated with the growth of cracks and is the result of the partial breakdown of the film at the anodes and the production of soluble anodic products that undermine the film. Up to point G in Figure 1, the general shape of the curves with stress is similar to that without stress; after this point the potential falls abruptly until fracture occurs at point F.

Electrochemical mapping[4] as stress-corrosion cracking is progressing, has clearly shown that the specimen surface is covered with anodic and cathodic areas and that the location of cracks is intimately connected with the strongly anodic zones.

From potential measurements, Hoar and Hines[5] proposed that the fracture of 18-8 type steels by stress-corrosion cracking involved two stages:

(1) A period of induction during which electrochemical processes lead to crack initiation.

(2) Crack propagation when crack growth is controlled by the anodic metal dissolution reaction at the advancing edge of the crack.

Their observations that crack propagation in stainless steel is slow relative to brittle fracture and that a growing crack can be stopped by

ARF 2152-18
(Final Report)

cathodic protection have led to the conception of a purely electrochemical mechanism of stress-corrosion cracking. This proposed mechanism has been criticized from many standpoints, and it has become increasingly apparent that the over-all mechanism of stress-corrosion cracking consists of two or more simultaneously active processes.

Potential vs time data, although valuable, are of limited usefulness since they tell little of the mechanical aspects of stress-corrosion cracking. For instance, the similarities in the curves in Figure 1 lead to the following conclusions:

(1) Potential measurements are insensitive to stress and strain. Differences between unstressed and stressed specimens only appear when new surfaces are rapidly being formed--i.e., during crack propagation.

(2) The similarity of the curves in Figure 1 during the induction period indicates that the role of stress during the early stages of the test is negligible. Indeed, van Rooyen[6] has suggested this and claimed that the time to fracture is not affected by the application of load some time after starting the test. Conversely, this similarity might reflect the inability of potential-time measurements to differentiate between some of the mechanical aspects of the phenomenon that occur during the induction period.

The electrochemical processes result in the generation of ions, but it has been demonstrated that cracking of 18-8 steels in magnesium chloride is not specifically due to chloride or magnesium ions; similar failure has been observed in a wide variety of chlorides. Furthermore, it has been shown that an aqueous solution is not even required for cracking, as a number of failures have been produced in boiling nitrobenzene.[4]

Some investigators[7] have considered the possible influence of certain critical ion species on the surface energy term associated with the fracture process. This is considered further in the next section.

B. **Mechanical Processes**

In addition to electrochemical considerations, there must exist the necessary mechanical conditions if cracking is to occur. The contribution made by mechanical processes is now discussed.

The influence of applied stress on the time to fracture for an 18-8 type steel in a variety of conditions in $MgCl_2$ is illustrated in Figure 2. An increase in stress is shown to result in a decrease in time to failure. A "knee" exists in the time to fracture-applied stress relationship due to the fact that at stress levels below about 0.1% proof stress there is a rapid increase in the time required to produce failure. This is particularly significant to the dislocation model of fracture since the engineering yield point (which is in the vicinity of the 0.1% proof stress) represents a stress level at which a transition occurs from limited to gross dislocation multiplication and subsequent interaction. If large numbers of dislocations are required for crack growth, therefore, it is to be expected that stress levels in the plastic range would be considerably more effective in producing failure than those in the elastic range.

Many investigators have claimed that the phenomenon of stress-corrosion cracking is mainly electrochemical, and many aspects of the possible role of dislocations in crack initiation and propagation have been

ARMOUR RESEARCH FOUNDATION OF ILLINOIS INSTITUTE OF TECHNOLOGY

- 7 -

ARF 2152-18
(Final Report)

neglected. In the extreme case, Hoar and West[8] suggested that the growth of cracks can occur entirely by anodic dissolution and that stress only acts to accelerate anodic dissloution at the tip of the crack due to the continual arrival of dislocations at the surface. However, there is considerable evidence indicating that mechanical processes and their manifestations are as essential to the phenomenon as the electrochemical contributions.

Cracks generated by stress-corrosion embrittlement have many features in common with brittle-type fracture often observed in bcc metals. Therefore, some aspects of current thinking on the basic mechanisms of brittle fracture in crystalline solids are now briefly reviewed since they are probably generally applicable to the formation of cracks under conditions of stress corrosion.

When crystalline solids are stressed, there is always the possibility that plastic deformation will occur, sometimes only to a very limited extent, by the glide of crystal dislocations. Although this possibility decreases as we move away from close-packed metallic crystals to ones of lower symmetry and toward low temperatures and rapid loading, it can hardly ever be disregarded. The general picture that we are concerned with, therefore, is one in which a number of glide dislocations are produced in a glide system by an applied stress. These dislocations pile up against a barrier such as a grain boundary and produce a stress concentration at the head of the pile-up. One of two possibilities can then occur:

(1) Operation of nearby Frank-Read sources leading to the propagation of plastic deformation and the relief of the stress concentration at the pile-up. In this case the metal is ductile.

(2) Conversion of glide dislocations into cavity dislocations which then spread and multiply in the form of a growing crack. In this case the metal is brittle.

This model is basic to most recent theoretical treatments of semi-brittle fracture in crystalline materials.

Cracking in 18-8 type steels is essentially transgranular. Therefore, if the formation of cracks is to be explained on the basis of dislocations piling up against barriers, these barriers must exist within the grains. Furthermore, in the case of stress-corrosion cracking, the barriers must be located along paths of chemical reactivity.

Robertson and Tetelman[9] have recently considered this problem and proposed that the sites of reaction are Cottrell-Lomer barriers and specifically the $\langle 110 \rangle$ sessile dislocations and the two stacking fault ribbons that lie at the intersection of two operating $\{111\}$ planes. These barriers are created by plastic deformation even at small plastic strains and their strength is primarily a function of the stacking fault energy which, in turn, is a function of the type and composition of the metal or alloy involved. The strength of the barrier is of importance since this dictates the number of dislocations that can be held in the pile-up and thus the magnitude of the stress concentration at its head. These issues are dealt with in detail by Robertson and Tetelman.[9]

However, even when obstacles do exist in ductile face-centered cubic lattices, the problem of producing cleavage still remains complicated. Theory suggests that the barriers in fcc metals are not strong (compared to bcc metals), and they alone cannot result in the generation of brittle-type cracks. At this stage, therefore, we must consider the possible influence that environment can have on the surface energy associated with crack growth. Surface energy is considered fundamental to the fracture process, and Cottrell has shown, theoretically, that cracks formed by dislocation coalescence will begin to spread when

$$\sigma nb \geqslant 2 \gamma$$

where σ is the shear stress on a glide plain, n is the number of dislocations in a pile up of Burgers victor b, and γ is the surface energy term. Environmental conditions can sometimes lead to a lowering of γ[10, 11] when the energy of a chemical reaction (γ_R) can contribute to the propagation of a crack. Thus, if γ_R is large, then $\gamma - \gamma_R$ will be small and the force required to advance a crack may become very small. This provides a mechanism, therefore, for the production of brittle type cracks in normally ductile material and has been suggested by some investigators[7, 9] to be an important factor in stress-corrosion cracking.

The role of surface energy was investigated experimentally by Coleman, Weinstein, and Rostoker[7] in the earlier part of this program. The approach was based upon the Stroh-Petch equation relating brittle fracture stress and grain size:[12, 13]

$$\sigma_F = \sigma_o + kd^{-1/2} \tag{1}$$

where σ_F = fracture stress, d = grain diameter; σ_o and k are constants of which

$$k = \sqrt{\frac{6\pi G \gamma}{1 - \nu}} \tag{2}$$

where G = modulus of rigidity; ν = Poisson's ratio; γ = surface energy associated with the formation of new surfaces in fracture. Specimens of 304 stainless steel and Mg-6% Al alloy were tested over a range of grain sizes in suitable stress-corrosion media and the values of k determined. The surface energy terms were subsequently derived from equation 2 (see Appendix). It was shown that the stress-corrosion environments had produced a lowering of the surface energies which could be related to the initiation of fracture in an environment known to produce stress-corrosion cracking. It was envisaged that certain critical ion species present in the environment were adsorbed at crack nuclei, resulting in a lowering of the surface energy associated with the fracture process.

In addition to studying the cracking behavior of fully softened materials, the influence of prior plastic strain on the time to failure of 18-8 alloys has also received some attention. Since prior plastic strain will change mechanical properties and microstructure, it should certainly be expected to influence cracking characteristics. Hoar and Hines[5] pre-strained specimens of 18-8 steel 8% (presumably at room temperature) and found that on subsequent testing in $MgCl_2$ the time to fracture was shortened (see Figure 2) and more cracks were produced compared with fully softened

ARMOUR RESEARCH FOUNDATION OF ILLINOIS INSTITUTE OF TECHNOLOGY

ARF 2152-18
(Final Report)

material. It was suggested that pre-straining increased the number of potential surface sites from which stress-corrosion cracks may be initiated and thus, at high stress particularly, decreased the necessary incubation period for the commencement of crack growth. They considered that crack initiation was probably favored by the presence of strain-induced martensite at the specimen surface.

The cracking of cold swaged 304 stainless steel in $MgCl_2$ was studied by van Rooyen[6] and, in agreement with Hoar and Hines, cold work was found to reduce the time to failure.

The results in Figure 3 after Hines[14] show the variation in time to fracture of an 18-8 Ti steel with amount of cold work; the data were obtained on specimens cold-worked by tensile loading. At 31,360 psi (just above the 0.1% proof stress of the fully softened alloy) cold work has little effect except at 15% and 30% pre-strain; also, there is some indication of a minimum at about 7%. However, at 11,200 psi the general trend, although the same, is far more pronounced. Thus at low levels of strain these data agree with previous work, [5] while at larger amounts of strain the behavior is reversed and the time to failure is observed to increase. Robertson and Tetelman point out that this behavior pattern is in accord with their proposed model for stress-corrosion cracking in stainless steels.

In some respects it is difficult to interpret this previous work since the pre-straining appears to have been carried out at room temperature. It is well known that, under such conditions, susceptible 18-8 alloys can be

readily transformed to strain-induced martensite. Thus, in addition to strain effects, observed behavior might have been significantly influenced by the presence of second phases in the microstructure. Furthermore, the variation in experimental results that appears in scattered data in the literature makes it impossible to clearly define the role of prior deformation on the stress-corrosion cracking behavior of stainless steels. This certainly represents an area where further research is required.

Reed and Paxton[15] made a study of stress-corrosion cracking of single crystals of a number of austenitic stainless steels to determine the crystallographic features of crack initiation and propagation. It was found that the crack plane in Fe-20Cr-20Ni specimens followed the (100) plane with the highest normal stress upon it. This was the first evidence of brittle cracks following a particular crystal plane in a fcc material. The 304 single crystals developed cracks roughly normal to the tensile axis, but there was no relationship between any crystallographic plane over long distances. Similar results were found for Fe-20Cr-12Ni single crystals. Furthermore, crack surfaces of the 304 crystals did not exhibit any structure which would associate the general crack surface with a particular crystallographic plane. The lack of microscopical evidence for crystallographically defined cracks in 304 stainless steel complicates the development of a model to account for the generation of cracks by dislocation coalescence in this material. However, there is evidence in other systems (e.g., Cu_3Au[16] and Fe-20Cr-20Ni[15] single crystals) which supports a dislocation mechanism for crack formation.

In the present study, work has been devoted partly to an examination of some of the effects of stress-corrosion cracking that remained unexplained from the earlier part of the program. Of particular interest has been the nature of crack growth and the interplay between exposure time (in both the absence and the presence of stress) and applied stress on crack propagation and ultimate specimen failure.

In addition, the study was extended to an investigation of the influence of thermal and mechanical history on stress-corrosion cracking in an effort to gain a better understanding of the influence of these parameters on the phenomenon. A commercial grade 304 stainless steel was used in all the experimental work.

IV. MATERIAL AND TESTING PROCEDURE

The investigation was confined to a study of commercial grade 304 stainless steel because previous work on this program had been performed on this material, the techniques for testing it had been established, and many aspects of the stress-corrosion phenomenon requiring further study were associated with its behavior.

The stainless steel was supplied in the fully softened condition in the form of 1 in. x 0.140 in. x 36 in. strips. The composition of the steel is shown in Table I, and its tensile properties at 140°C (exposure temperature to $MgCl_2$) are listed in Table II. Specimens for the stress-corrosion experiments were cut using a standard Tensil-Kut fixture to give strip specimens

as shown in Figure 4. Tensile properties were determined on strip specimens shown in Figure 5; these specimens were prepared by milling.

The over-all length of the stress-corrosion specimens was 12 in., allowing them to be gripped outside the $MgCl_2$ solution. This avoided spurious electrochemical effects which could arise if grips of a dissimilar metal were submerged in the aqueous solution. After cutting the gage lengths, the cut edges were carefully hand filed and polished with 240-grit silicon carbide paper to a smooth finish to remove any gross working effects introduced during cutting. This was found to be particularly important in the preparation of specimens that had received prior deformation.

Strip specimens were chosen for this study since the rectangular cross-section made possible an accurate determination of crack growth. The geometry of wire specimens is not suited for this purpose.

After polishing, specimens were degreased in acetone and placed in the rig shown in Figure 6. A 42w/o $MgCl_2$ solution, previously prepared by adjusting the boiling point to 154°C, was poured into the glass test cell (500 ml capacity), around which was wrapped a heating element. The temperature in the cell was controlled at 140° ± 1°C throughout the experimental work. This temperature was chosen because it was below the boiling point of the solution and would thus minimize compositional changes in the solution during extended testing. To prevent corrosion at the air-liquid interface, the upper portion of each specimen was coated with an epoxy resin which was stable in the $MgCl_2$ environment.

ARMOUR RESEARCH FOUNDATION OF ILLINOIS INSTITUTE OF TECHNOLOGY

ARF 2152-18
(Final Report)

The rig shown in Figure 6 is part of a dead-weight loading creep testing unit modified for stress-corrosion testing. Stress was applied to the specimen through a simple loading arm system where the loading pan was slowly released by a manually controlled air jack. The length of the arm was such as to give about a 20:1 loading ratio. The extension of the specimen was measured to within 0.001 in. from a dial gage attached to the frame of the testing unit (see Figure 6). The time to fracture was automatically recorded by a suitable electric timer-microswitch circuit.

It was recognized at the beginning of the program that minor variations in the composition of $MgCl_2$ can result in small but significant differences in the cracking behavior of a given grade of susceptible steel. Furthermore, during extended testing, $MgCl_2$ solutions do undergo compositional changes. Consequently, in order to avoid the influences of these changes on test data, all the $MgCl_2$ used in this program was obtained from the same batch and each solution was not used for more than two tests. Each test was limited to a maximum duration of about 100 hours; if the specimen had not failed in this time, it was removed from test.

All metallographic samples were prepared by standard polishing techniques and electrolytically etched in an aqueous solution of chromic acid.

V. RESULTS AND DISCUSSION

A. Tensile Tests

Some tensile tests on fully softened, as-received material were carried out at 140°C both in air and in $MgCl_2$. The specimens were tested on an Instron machine employing a cross-head speed of 0.02 in/min--i.e., strain rate of $2.4 \times 10^{-4} sec^{-1}$. The load-elongation relationships obtained are shown in Figure 7, and the yield and fracture data are listed in Table II. The results indicate that the behavior of polycrystalline 304 stainless steel during the early stages of plastic deformation is identical for both environments, and there is no evidence of the Roscoe Effect or Rebinder Effect. However, the ultimate tensile strength and elongation are appreciably reduced by the presence of $MgCl_2$; this is due to stress-corrosion cracking that occurred during the test. Obviously, the extent to which the ultimate tensile strength is lowered in the $MgCl_2$ environment will depend sensitively on the strain rate used in the test.

B. Influence of Applied Stress

The influence of applied stress on the stress-corrosion cracking of as-received, fully softened 304 stainless steel was studied in the stress range 30,000-50,000 psi. In all cases the holding time in $MgCl_2$ prior to the application of stress (t_o) was 15 min. In these experiments, measurements of time to fracture, specimen extension with time, and rate of crack growth were made. These data are summarized in Tables III and IV and in Figures 8, 9, and 10.

ARMOUR RESEARCH FOUNDATION OF ILLINOIS INSTITUTE OF TECHNOLOGY

ARF 2152-18
(Final Report)

The influence of applied stress (σ) on time to fracture (t_f) gives a linear relationship on semi-logarithmic graph paper, indicating that within this stress range an equation of the following form is obeyed:

$$t_f = c \log \sigma$$

where c is a constant.

A similar type of relationship was observed by Hoar and Hines[2] for a series of stainless steels tested in $MgCl_2$.

The extension-time data obtained at different initial applied stresses are given in Figure 9. The general form of the curves is similar to the familiar creep curves observed under constant loading conditions.

To measure crack growth, two series of specimens were sectioned and metallographically examined after various time intervals between initial loading and ultimate fracture. These data, obtained at 35,000 and 50,000 psi, are plotted in Figure 10 along with their respective time-extension curves. The results indicate that specimen extension is directly related to crack growth and that the time to fracture may be divided into three stages:

(1) The first stage represents the initial extension of the specimen on loading due to elastic-plastic strain.

(2) During the second stage, the rate of extension decreases; this is most pronounced at the lower stress levels. This stage represents a period of crack nucleation and initial growth. Since crack growth appears to commence very soon after stress has been applied, the incubation period observed by Hoar and Hines[5] and others is either non-existent or extremely short. The length of this stage decreases with increasing applied stress suggesting that stress has a significant influence on the time required to initiate cracking.

ARF 2152-18
(Final Report)

(3) In the third and final stage the rate of extension increases
rapidly and is attributed to the reduction in effective load-
carrying cross-section as a consequence of crack growth.
As a result of this extension, the specimen core is subjected
to considerable plastic strain as the true stress increases
rapidly above its initial value. Under these conditions of con-
stant load, ultimate failure is governed by the tensile strength
of the metal and the applied load. The rate of extension and
rate of crack growth (~2.4 mm/hour) in this stage reach a
maximum which appears to be relatively insensitive to the
initial applied stress. The value of 2.4 mm/hr compares
with a rate of crack growth of 1 to 4 mm/hr quoted by Hoar
and Hines.[5]

The results demonstrate that in these stress-corrosion experiments,
the stage during which crack growth occurs is long, while the incubation
period which precedes crack nucleation is extremely short. These findings
are in direct contrast to the interpretation given to potential-time data
accumulated by previous investigators.[3,5]

No discontinuous flow was observed in any of the extension measure-
ments, suggesting that crack growth occurred at a uniform rate. However,
if crack growth was, in fact, rapid and discontinuous, the steps were very
small and could not be detected by the measuring techniques employed.

Metallographic examination of specimens indicated that crack growth
was uniform on all four faces and all cracks appeared to grow at the same
rate. Cracking was also observed to be essentially transgranular as
illustrated in Figure 11.

The crack patterns produced at the various stress levels are
illustrated in Figures 12 to 14, and show that cracks were essentially per-
pendicular to the direction of applied stress. Furthermore, crack density

ARMOUR RESEARCH FOUNDATION OF ILLINOIS INSTITUTE OF TECHNOLOGY

ARF 2152-18
                                                    (Final Report)

increased with increasing applied stress and was most marked between 30,000 and 40,000 psi.

Prestressing specimens in air at 140°C before adding the $MgCl_2$ solution had no influence on the time to fracture or the nature of the crack patterns. The latter observation differs from the work of Reed and Paxton[15] on single crystals of Fe-20Cr-20Ni; these investigators noted that specimens strained in $MgCl_2$ solution developed many more cracks than those specimens that were prestrained in air.

C. Influence of Holding Time in $MgCl_2$ and Air on Time to Fracture

The existence of an induction time for cracks to initiate when stressed austenitic steel is exposed to $MgCl_2$ has been noted by several investigators. Hoar and Hines,[5] in a study of stainless steels, observed that this induction time decreased with applied stress and with the addition of HCl to the $MgCl_2$. Experiments on clean and pre-oxidized specimens indicated that the delay was due to the time necessary for surface oxide films to be broken down by the $MgCl_2$ solution. In agreement with the work of Barnartt and van Rooyen,[3] these investigators found that the potential-time curves for this crack-susceptible material was little influenced by stress up to a few minutes before a wire fractured. Furthermore, van Rooyen[6] has claimed that the time to fracture is not affected if the load is applied some time after the start of a test. To investigate this behavior further, a series of experiments was carried out and is described below.

The influence of holding time in MgCl$_2$ and in air at 140°C on the subsequent time to fracture under an applied stress in MgCl$_2$ at 140°C has been studied. The results are summarized in Table V. These data indicate that varying the holding time in MgCl$_2$ or air from 0 to 960 minutes had no influence on the subsequent time to failure at either of the stress levels investigated. However, a change was noted in the crack patterns on specimens held for 960 minutes in MgCl$_2$, as can be seen from a comparison of Figures 14 and 15. The crack density for the specimens subjected to the extended holding time was considerably reduced although the time to failure remained essentially the same. The reduction in the number of surface cracks may have been due to the formation of localized passive films on the specimen surfaces during holding.

The present results are not in agreement with previous work from two standpoints. Firstly, the results throw doubt on the supposed role of an oxide or passive film in determining time to failure by stress-corrosion cracking. A similar conclusion was reached in recent work by Uhlig and Sava,[17] who examined the cracking behavior of 310 stainless steel. Secondly, the failure time is governed by the time at stress rather than the actual over-all time in the stress-corrosion environment. Thus any change in potential that takes place while in the unstressed condition does not appear to contribute to the subsequent cracking kinetics of stressed specimens. Therefore, although the potential-time data collected during the early stages of exposure are similar for unstressed and stressed specimens (up to G in

Figure 1), there must be a marked difference in the actual sequence of events that accompany this change in potential. In the unstressed material nothing that contributes to the cracking process seems to occur, whereas in stressed specimens crack nuclei must form during this period. It is concluded that potential-time measurements are unable to differentiate between these two quite different courses of events. These findings illustrate the difficulty of separating the contributions made by electrochemical and mechanical behavior to the stress-corrosion cracking phenomenon--a problem that continually plagues investigators in this field of research.

The specimens exposed to air at 140° C were stressed throughout the holding period for two reasons:

(1) The oxide film formed during holding would not be damaged by subsequent stressing.

(2) The plastic strain introduced by the applied stress would accelerate any possible aging processes that might occur in the austenite during holding.

Since the test data (see Table V) indicated that pre-exposure to air did not influence the time to fracture, it was concluded that these factors were not significant enough to influence cracking behavior. The aging effects noted by Uhlig and Sava[17] on a type 310 stainless steel were not observed in the present work.

D. Influence of Prestressing Temperature

To study the influence of the temperature of stressing on subsequent stress-corrosion cracking behavior at 140°C in $MgCl_2$, a series of specimens

ARMOUR RESEARCH FOUNDATION OF ILLINOIS INSTITUTE OF TECHNOLOGY

ARF 2152-18
(Final Report)

were prestrained in air in the range 140° -500°C. All specimens were loaded to an initial stress of 50,000 psi (determined from the original cross-sectional area), were measured for elongation, and were subsequently exposed to $MgCl_2$ at 140°C without changing the load on the specimen. Under this procedure, the initial applied stress in $MgCl_2$ varied for each specimen, being greater for higher prestressing temperature.

The prestressing temperature-per cent elongation and prestressing temperature-time to failure results are given in Figure 16. They indicate that the per cent elongation and time to failure both increase with prestressing temperature, and the similar trends of these two curves suggest that time to failure is very sensitive to the amount of prestrain. Thus increasing amounts of prestrain in the range 10-18% result in a fivefold increase in the time to failure. The role of temperature in these experiments is thought to be confined solely to producing varying amounts of prestrain which harden the steel and thus raise its yield stress for subsequent testing at 140°C. Examination of specimens after failure indicated that prestressing above 140°C resulted in a marked decrease in crack density. This is illustrated by comparing Figures 14 and 17.

The reduced susceptibility of 304 stainless steel to cracking with increasing prestrain is attributed to:

(1) Increased difficulty of nucleating cracks in worked material.

(2) Presence of large numbers of slip bands which act as barriers to crack propagation. Since the slip band density is proportional to the amount of prestrain, it is to be expected that susceptibility decreases with prestrain.

ARMOUR RESEARCH FOUNDATION OF ILLINOIS INSTITUTE OF TECHNOLOGY

- 23 -   ARF 2152-18
                                          (Final Report)

E. Influence of Cyclic Loading on Crack Propagation

In the work described in the Appendix, brittle cracks were observed to be readily initiated in 304 stainless steel on continuously loading in a $MgCl_2$ environment. However, it was noted that these cracks did not propagate very far even at the higher stress levels. These data, in conjunction with values determined for surface energy, suggested that cracks may have formed rapidly as do normal brittle cracks and that propagation was governed by the rate of supply of certain adsorbing ion species to the root of the crack. If this is the case, we would anticipate that cyclic loading will influence the time at stress required to produce failure in the following way:

(a) After the application of stress to a specimen immersed in $MgCl_2$, brittle cracks form at the surface of the specimen, but their continued growth is delayed due to the absence of the necessary adsorbed ions at the newly formed crack roots.

(b) After a time interval, ions diffuse to and become adsorbed at the new crack roots which are then conditioned to allow further crack propagation in the presence of stress. It is envisaged that the processes that occur during this time interval, as van Rooyen[6] suggested for the incubation period for crack initiation, do not require the presence of stress.

(c) The next stage involves further, but limited, stress-activated crack growth. Crack growth is again delayed, and the complete sequence of events described in (b) is repeated. This picture suggests that stress is only effective for part of the time during a stress-corrosion test in producing crack growth. Under conditions of cyclic loading, therefore, we would expect the integrated time at stress necessary to produce fracture to be less than that under conditions of constant loading.

To examine the validity of this model, cyclic loading experiments were carried out and are described below.

ARMOUR RESEARCH FOUNDATION OF ILLINOIS INSTITUTE OF TECHNOLOGY

ARF 2152-18
(Final Report)

A series of cycling conditions was studied; these are illustrated in Figure 18, while extrusion-time data for one of the experiments are given in Figure 19. The times to failure at the different applied stress levels and cycling conditions are summarized in Table VI.

The results indicate that the integrated time at stress to produce fracture was not significantly influenced by any of the cycling schedules used and these times were essentially the same as observed in the constant loading experiments. Specimens subjected to the F cycling treatment (see Figure 18) did show some reduction in time to failure, but this was thought to be due to the repeated loading of the specimens during cycling. The load was applied by the slow release of an air jack, but the motion of the loading pan at the instant of complete release, although quite small, would tend to make the effective load slightly greater than the true load. Thus the specimen would experience a small instantaneous increase in stress at the start of each cycle which would produce a small additional extension. Such an effect would tend to accelerate failure but would only be significant when a large number of cycles were involved, as in schedule F in Figure 18.

These results indicate that the growth of cracks during stress-corrosion cracking requires the simultaneous aid of both mechanical and electrochemical processes. Furthermore, cracks appear to grow slowly rather than abruptly. This is demonstrated by the curve in Figure 20, which shows the extension-time relationship of a specimen during a four-minute period at 40,000 psi (peak A in Figure 19). Extension, which is interpreted

as a measure of crack growth, is slow when the specimen is initially re-loaded; the rate gradually increases with time, reaching a constant value between the second and fourth minutes. No jumps in extension were observed. It appears, therefore, that in addition to stress, a stress-induced electro-chemical condition has to return before crack growth can proceed at the normal rate. If crack propagation occurred by a mechanism of alternating steps of brittle fracture as suggested earlier, the extension-time relation-ship would be expected to be of the form given by the broken curve in Figure 20. However, the reverse effect was observed. It is concluded that in 304 stainless steel, stress-corrosion cracks propagate slowly and are the result of the simultaneous co-operative action of mechanical and electro-chemical phenomena.

F. Influence of Prior Deformation and Microstructure

The influence of microstructural changes in 18-8 type stainless steel, brought about by variations in thermal and mechanical histories, on stress-corrosion cracking behavior has not been thoroughly studied. Further-more, available data are, in some respects, conflicting. A further examina-tion has been made, therefore, in which 304 stainless steel was subjected to the following treatments:

(A) Water quenched from 982°C (1800°F) and rolled at 300°C

(B) Furnace cooled from 982°C (1800°F) and rolled at 300°C

(C) Water quenched from 982°C (1800°F), rolled at 300°C
     and subsequently annealed at 700°C for 168 hours.

(D) Water quenched from 982°C (1800°F) and rolled 15% in
     the temperature range 23° to -196°C

ARMOUR RESEARCH FOUNDATION OF ILLINOIS INSTITUTE OF TECHNOLOGY

ARF 2152-18
                                      (Final Report)

These treatments produced a variety of microstructures, a selection of which is shown in Figures 21 to 25. The rolling at 300°C was carried out to prevent the formation of strain-induced martensite even at reductions up to 50%. The furnace-cooled and 700 °C annealed samples contained significant amounts of precipitated carbides, and the depletion in the carbon content of the austenite made the latter more susceptible to strain-induced transformation. However, specimens subjected to treatments (A), (B), or (C) did not contain martensite prior to testing. The rolling in treatment (D) was performed at 23°, -50°, and -196° C where the subzero temperatures resulted in the transformation of some of the austenite to martensite. In this series of specimens the amount of prestrain was held constant while the austenite/martensite ratio was varied.

The tensile properties at 140 °C and the time-to-failure data for these materials are listed in Tables VII to XII and plotted in Figures 26 to 29. The tensile data were collected in order to relate observed stress-corrosion behavior with corresponding strength characteristics. Most of the time-to-failure tests were carried out at applied stresses of 40,000 and 75,000 psi. The final thickness of the stress-corrosion test specimens was, in all cases, 0.070 in. Since specimen thickness does influence time to failure results, this step made all results directly comparable from the standpoint of specimen geometry. However, it should be noted that in all the experiments carried out in the previous sections, the specimen thickness used was 0.140 in.

ARMOUR RESEARCH FOUNDATION OF ILLINOIS INSTITUTE OF TECHNOLOGY

ARF 2152-18
(Final Report)

Initial experiments on rolled specimens showed that crack nucleation was almost entirely confined to the two narrow edges of the specimen gage length. The existence of these preferred sites suggested that the cutting of the gage length left edges which were particularly sensitive to cracking. This was found to be the case when, by more careful and lengthy preparation of specimens, time-to-fracture values were increased considerably. Furthermore, the crack patterns on these specimens were more uniform than those observed in the initial tests. This more careful preparation, which involved hand filing and polishing with emery paper, was used, therefore, in all subsequent tests.

The time to failure-0. 5% proof stress data for specimens given treatments (A), (B), and (C) at two applied stress levels are given in Figure 29. The results indicate that increasing the applied stress leads to a reduction in the time to failure and, as the applied stress falls below the proof stress of the material, the time to failure shows a sharp increase. This behavior pattern is very similar to that exhibited by fully softened specimens.

An interesting feature of the data is that the curves at 40,000 psi show a maximum which is not as apparent at 75,000 psi. A similar maximum was observed by Hines[14] on a susceptible stainless steel at a stress level of 31,360 psi. The initial increase in time to failure at both stress levels can be explained, in part, by the fact that as the amount of pre-strain by rolling increases, the applied stress falls below the proof stress of the specimens. In terms of a dislocation model where crack growth is governed

ARF 2152-18
(Final Report)

by the generation of dislocations, it is visualized that purely elastic stresses would not be very effective in promoting crack propagation. Thus in those cases where the applied stress falls below the proof stress of the material, crack growth is slow until the cross-section of the specimen has been reduced enough for the applied load to cause plastic deformation. At this stage cracks grow more rapidly, leading to ultimate failure. The observations made by Edeleanu [18] indicate that the slip bands introduced during prestraining would also help to increase the time to failure since they act as barriers to crack propagation.

The falling off in the time to failure as the proof stress is increased by prior rolling may be attributed to residual stress effects. Hundy [19] showed that, except for extremely light reductions, the surface residual stresses in rolled mild steel were tensile and increased in magnitude with reduction. The presence of such stresses in the present experiments would have an additive effect and would result in the actual surface stresses being considerably higher than the applied stress. Thus crack formation would be accelerated, and the material would exhibit an increased susceptibility to stress-corrosion cracking. However, this does not explain the behavior of 700°C annealed specimens which should be essentially free from internal stress.

There is a considerable difference in the susceptibilities of the different structures at 40,000 psi, while at 75,000 psi they follow the same general trend except for treatment (c) at a proof stress of 51,000 psi. The

ARF 2152-18
(Final Report)

results indicate that at 40,000 psi, the duplex austenite + carbide structures, where the austenite is depleted in carbon and chromium content, are superior to single-phase austenite both in the softened and worked conditions. It is doubtful that the change in austenite chemistry can explain these results since van Rooyen[20] recently reported that the resistance of austenitic stainless steels to transgranular stress-corrosion cracking was increased with solute carbon concentration. The physical presence of carbides or the fact that the austenite depleted of carbon undergoes strain-induced transformation during testing could possibly explain the observed differences in susceptibility. However, metallographic evidence of cracked specimens does not support either of these possibilities. The structures in Figure 11 and Figures 22 to 25 show that cracking is, in general, transgranular and the nature of the cracks is similar in all structures. It was noted that some intergranular cracking did occur in rolled material (see Figure 25) due, perhaps, to the reduced susceptibility of the grains as a result of prior deformation. The precipitation of large amounts of carbides at grain boundaries in treatments (B) and (C) did not appear to influence the intergranular type of cracking (see Figures 22 to 24) characteristic of the fully softened material (Figure 11).

The specimens produced by treatment (D) had the greatest resistance to stress-corrosion cracking of any of the materials tested. The results indicate that the lower the temperature of deformation, the stronger the material and the less susceptible it became to cracking. In order to deter-mine whether it was the increase in strength or the presence of strain-

induced martensite that conferred the improved cracking resistance, a series of specimens containing varying amounts of martensite was tested at a constant applied stress/fracture stress ratio of 0.83. The results given in Table XII clearly indicate that it was the martensite that imparted the improved resistance to cracking. These findings are in agreement with previous resulted reported by Edeleanu.[21]

The fact that martensite improves resistance to stress-corrosion cracking is somewhat surprising if we consider crack formation in terms of the Stroh-Cottrell dislocation model. On these grounds we would expect a body-centered type structure such as martensite to be more susceptible to the generation of brittle type cracks than face-centered cubic austenite. Furthermore, the formation of martensite from austenite is a diffusionless transformation where no change in chemistry is involved. Thus the same chemically reactive sites should exist in the duplex structures as were present in fully softened material, and it is at these sites that cracks are considered to nucleate and propagate. Obviously, many of these sites must become inoperative in the presence of martensite. Edeleanu[21] suggested that corrosion becomes rather generally distributed in the presence of martensite; this results in a less dangerous form of attack and thus an enhanced resistance to cracking.

It is suggested that the difference in susceptibility between austenite and martensite lies in their different crystallographic structures and in the fact that stacking faults are present in the former but not the latter.

ARMOUR RESEARCH FOUNDATION OF ILLINOIS INSTITUTE OF TECHNOLOGY

ARF 2152-18
(Final Report)

It was noted that prior deformation considerably reduced the number of surface cracks present in fractured specimens. This is illustrated in Figure 30 and parallels the behavior of specimens pre-stressed at temperatures above 140°C and subsequently tested at 140°C (section D). The mechanism that controls crack density remains unexplained although it represents a vital aspect of stress-corrosion cracking.

There is an increasing amount of evidence which indicates that the factors influencing crack nucleation require further study. The weakest point in all theories of stress-corrosion cracking advanced by prior investigators lies in this initial period of the cracking process. This is a direct reflection of our lack of knowledge of the events that occur during this stage.

In an effort to gain a better understanding of the fracture mechanism, a series of fracture faces was examined under the light microscope. The irregular river pattern structures illustrated in Figures 31 and 32 were most frequently observed and were characteristic of both fully softened material and specimens produced by treatments (A), (B), and (C). The structure in Figure 33 was less frequently seen and appears to be a typical cleavage type fracture. However, it may represent a grain boundary area where limited intergranular cracking occurred.

The irregular fracture patterns observed in the austenitic specimens (Figures 31 and 32) were not detected in the martensitic structures (treatment (D)--rolling at -196°C). These fracture surfaces were heavily tarnished; consequently, little could be seen under the microscope. However, the

ARMOUR RESEARCH FOUNDATION OF ILLINOIS INSTITUTE OF TECHNOLOGY

brittle type fracture shown in Figure 34 was noted in isolated areas. This fracture may be due to stress-corrosion cracking processes or could be attributed to purely mechanical cleavage caused by the interaction of the applied stress and a nearby notch (i.e., crack) formed at an earlier stage by stress-corrosion.

Although the above findings are not conclusive, the evidence of cleavage cracks does support the contention that a brittle fracture mechanism may be involved in the stress-corrosion cracking phenomenon.

VI. CONCLUSIONS

The following conclusions are based on the experimental results collected in this study:

(1) Tensile data on fully softened 304 stainless steel indicate that deformation behavior in the vicinity of the yield point is the same for specimens tested in air or in $MgCl_2$ at 140 C. It is concluded that polycrystalline material does not exhibit the Rebinder Effect or the Roscoe Effect.

(2) Increasing the applied stress decreased the time to failure and increased the crack density of fully softened 304 stainless steel tested in $MgCl_2$. The maximum observed crack growth rate was 2.4 mm/hr. Extension measurements of specimens under test were shown to directly reflect the rate of crack growth.

ARF 2152-18
(Final Report)

(3) The incubation period associated with a pre-cracking stage and observed by Hoar and Hines was not detected at the stress levels used in this study. Cracking was observed to commence almost immediately after the specimen was stressed.

(4) Varying the holding time, either in $MgCl_2$ at 140 C, prior to stressing had no effect on the subsequent stress-induced time to failure. The data suggested that thin oxide films on the metal surface had no influence on cracking behavior and the time to failure was governed solely by the time at stress.

(5) Prestressing at various temperatures at 50,000 psi prior to testing at 140 C in $MgCl_2$ indicated that the influence of prestressing temperature on time to failure was basically due to strain effects. The greater the amount of pre-strain, the longer the time to failure. The results did not suggest that structural or compositional changes caused during prestressing had influenced stress-corrosion behavior.

(6) Cyclic loading treatments were found to have no influence on the time to failure. In all cases, the integrated time at stress to produce failure was approximately the same as in the static fatigue tests. The results suggest that the transgranular cracking of 304 stainless steel requires the simultaneous participation of mechanical and electrochemical phenomena if cracks are to propagate.

(7) In agreement with previous work, there was no evidence of rapid crack propagation characteristic of brittle fracture.

ARMOUR RESEARCH FOUNDATION OF ILLINOIS INSTITUTE OF TECHNOLOGY

ARF 2152-18
(Final Report)

(8) Prior deformation at 300°C was shown to increase the time to failure of specimens subsequently tested at 40,000 and 75,000 psi in $MgCl_2$. Although a maximum was observed in the time to failure-0.5% proof stress curve at 40,000 psi, in no case was the time to failure observed to fall below that for unworked specimens.

(9) Prior deformation resulted in a marked reduction in the density of surface cracks generated on subsequent testing.

(10) Duplex austenite-carbide structures were considerably less susceptible to stress-corrosion cracking than the single-phase austenite both in the softened and worked conditions at an applied stress of 40,000 psi. However, at 75,000 psi these structures exhibited similar behavior.

(11) Structures containing strain-induced martensite were the most resistant of all the materials tested. The enhanced behavior was attributed to the difference in crystallographic structure between austenite and martensite.

(12) Fractographs of tested specimens revealed the presence of cleavage type fracture faces. This evidence supports the view that stress-corrosion cracks form by a brittle fracture type mechanism.

(13) The results of this study indicate that the mechanism of intergranular stress-corrosion cracking in 304 stainless steel depends on the simultaneous action of electrochemical and mechanical processes and the complex interplay that exists between them. Attempts have been made to separate the individual contributions made by these processes but have proved unsuccessful.

ARMOUR RESEARCH FOUNDATION OF ILLINOIS INSTITUTE OF TECHNOLOGY

ARF 2152-18
(Final Report)

The data do not appear to particularly favor either the predominance of an electrochemical mechanism or a mechanical mechanism suggested by previous investigators.

VII. LOGBOOKS AND CONTRIBUTING PERSONNEL
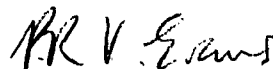
Data for this report are recorded in ARF logbooks C 10606 and C 11512.

The following personnel have been the principal contributors to the planning and execution of this work.
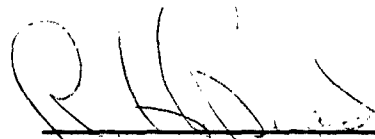
Oswald Sanders	Project Technician
J. R. Dvorak	Metallography
R. F. Dragen	Metallography
P. R. Evans	Project Engineer
R. H. Read	Supervisor

Respectfully submitted,

ARMOUR RESEARCH FOUNDATION OF
ILLINOIS INSTITUTE OF TECHNOLOGY

P. R. V. Evans
Research Metallurgist

Robert H. Read
Supervisor
Physical Metallurgy

R. J. Van Thyne
Assistant Director
Metals and Ceramics Research

REFERENCES

1. Hugh L. Logan, J. Research Nat. Bur. Standards, 61, 503, (1958).

2. T. P. Hoar and J. G. Hines, J. Iron Steel Inst., 184 (2), 166 (1956).

3. S. Barnartt and D. van Rooyen, Westinghouse Research Laboratories Scientific Paper 6-40807-13-P5, June 1960.

4. J. M. Miller and H. T. Francis, ARF Report No. 2181-12, "The Mechanism of Stress Corrosion in Stainless Steel."

5. T. P. Hoar and J. G. Hines, Stress Corrosion Cracking and Embrittlement, edited by W. D. Robertson, 1956 (New York: J. Wiley & Sons Inc.)

6. D. van Rooyen, Corrosion, 16 (9), 421 t, (1960).

7. E. G. Coleman, D. Weinstein and W. Rostoker, Acta Met., 9, 491 (1961).

8. T. P. Hoar and J. M. West, Nature (London), 181, 835 (1958).

9. W. D. Roberston and A. S. Tetelman, Office of Naval Research Contract Nonr 609 (28) Tech. Report No. 2, December, 1960.

10. J. J. Gilman, Fracture, p. 193, 1959 (New York: J. Wiley & Sons).

11. W. Rostoker, J. M. McCaughey, and H. Markus, Embrittlement by Liquid Metals, 1960 (Reinhold Publishing Co., New York).

12. N. J. Petch, Phil. Mag., (8) 1, 186 (1956).

13. A. N. Stroh, Advances in Physics 6, 418 (1957).

14. J. G. Hines, Physical Metallurgy of Stress Corrosion Fracture, p. 116, 1959 (Interscience, New York).

15. R. E. Reed and H. W. Paxton, Office of Naval Research, Contract Nonr 760 (14) NR 036-029, October 1960.

16. R. Bakish, Trans. AIME 209, 494 (1957).

17.   H. H. Uhlig and J. P. Sava, Office of Ordnance Research, Contract No. DA-19-020-ORD-5247, AD No. 251046.

18.   C. Edeleanu, Physical Metallurgy of Stress Corrosion Fracture, p. 79, 1959 (Interscience, New York).

19.   B. B. Hundy, J. Iron Steel Inst., 179, p. 23, January 1955.

20.   D. van Rooyen, Westinghouse Research Laboratories, Tech. Report No. 3 on Contract Nonr-2868 (00), NR 036-044/2-26-59.

21.   C. Edeleanu, Stress Corrosion Cracking and Embrittlement, edited by W. D. Robertson, 1956 (New York, J. Wiley & Sons Inc.)

TABLE I

CHEMICAL COMPOSITION OF THE 304 STAINLESS STEEL

Element	Concentration (weight per cent)
Carbon	0.06
Chromium	18.36
Nickel	9.08
Manganese	1.05
Sulfur	0.013
Phosphorus	0.025
Molybdenum	0.18
Silicon	0.50
Aluminum	0.006

TABLE II

TENSILE PROPERTIES OF THE 304 STAINLESS STEEL AT 140°C

Tensile Property (psi)	Testing Environment	
	Air	MgCl$_2$
Elastic Limit	22,400	--
0.05% Proof Stress	26,800	--
0.10% Proof Stress	28,500	--
0.5% Proof Stress	32,300	31,000
Ultimate Tensile Strength	70,100	60,500

TABLE III

INFLUENCE OF APPLIED STRESS ON TIME TO FAILURE
FOR 304 STAINLESS STEEL STRESSED IN $MgCl_2$ AT 140°C

Applied Stress (psi)	Holding Time in $MgCl_2$ (min)	Time to Fracture (min)
30,000	15	247
30,000	15	272
30,000	15	290
35,000	15	180.5
40,000	15	145
40,000	15	124
50,000	15	70
50,000	15	63
50,000	15	68

ARF 2152-18
(Final Report)

TABLE IV

VARIATION OF AVERAGE CRACK DEPTH WITH TIME

FOR 304 STAINLESS STEEL

STRESSED IN $MgCl_2$ AT $140°$ C

Applied Stress (psi)	Average Crack Depth (mm)	Time at Stress (min)
35,000	0.07	25
35,000	0.27	112
35,000	1.05	150
35,000	1.90	170
50,000	0.03	5
50,000	0.19	30
50,000	0.32	43
50,000	0.51	61

TABLE V

INFLUENCE OF HOLDING TIME IN $MgCl_2$ AND AIR

ON THE TIME TO FRACTURE OF 304 STAINLESS STEEL

Holding Time (min)	Environment During Holding Time	Applied Stress (psi)	Time to Fracture (min)
0	$MgCl_2$ at 140°C	40,000 [a]	140
0	$MgCl_2$ at 140°C	40,000 [a]	135
15	$MgCl_2$ at 140°C	40,000 [a]	122
15	$MgCl_2$ at 140°C	40,000 [a]	145
120	$MgCl_2$ at 140°C	40,000 [a]	140
480	$MgCl_2$ at 140°C	40,000 [a]	130
960	$MgCl_2$ at 140°C	40,000 [a]	158
15	$MgCl_2$ at 140°C	50,000 [a]	70
960	$MgCl_2$ at 140°C	50,000 [a]	81
4*	Air at 140°C	40,000 [b]	122
60*	Air at 140°C	40,000 [b]	143
975*	Air at 140°C	40,000 [b]	120

* $MgCl_2$ at 140°C was added immediately at the end of the holding period.

(a) Stress applied at end of holding period.

(b) Stress applied at beginning of holding period.

ARF 2152-18
(Final Report)

TABLE VI

INFLUENCE OF CYCLIC LOADING ON TIME TO FAILURE
OF 304 STAINLESS STEEL STRESSED IN $MgCl_2$ AT 140° C

Stress Range (psi)	Type of Cycling Treatment (see Fig. 18)	No. of Cycles	Integrated Time to Failure (min)
0-40,000	--	0	135[*]
0-40,000	A	2	165
0-40,000	A	2	158
0-40,000	A	2	146
0-40,000	B	2	141
0-40,000	C	2	130
0-40,000	D	2	145
0-50,000	--	0	67[*]
0-50,000	E	17	63
0-50,000	F	27	50
0-50,000	F	27	54

[*] Mean value of results given in Table III.

ARF 2152-18
(Final Report)

TABLE VII

TENSILE DATA ON HEAT TREATED AND ROLLED

304 STAINLESS STEEL TESTED IN AIR AT 140°C

% Reduction*	W.Q. from 982°C & Rolled at 300°C		Furnace Cooled from 982°C & Rolled at 300°C		W.Q. from 982°C, Rolled at 300°C, & Annealed at 700 C for 168 hr	
	0.5% Proof Stress (psi)	Fracture Stress (psi)	0.5% Proof Stress (psi)	Fracture Stress (psi)	0.5% Proof Stress (psi)	Fracture Stress (psi)
0	32,770	80,670	21,900	75,700	29,200	77,300
7	ND+	ND	50,000	79,400	ND	ND
10	67,510	87,760	ND	ND	45,300	81,200
20	83,450	96,800	ND	ND	53,700	85,300
27	ND	ND	84,300	100,400	ND	ND
30	92,050	105,990	ND	ND	69,000	95,000
44	ND	ND	101,800	119,100	ND	ND
50	103,060	122,560	ND	ND	64,000	96,300

* % Reduction determined from the relationship, % red = $\dfrac{h_o - h_f}{h_o} \times 100$

where h_o = initial thickness and h_f = final thickness of the strip.

+ ND - Not determined.

TABLE VIII

TENSILE DATA OF HEAT TREATED 304 STAINLESS STEEL

ROLLED 15% AND TESTED IN AIR AT 140°C

Rolling Temperature (°C)	Tensile Properties	
	0.5% Proof Stress (psi)	Fracture Stress (psi)
+60	54,286	90,000
÷23	54,286	91,429
-50	63,888	121,666
-196	79,096	151,977

TABLE IX

TIME-TO-FAILURE DATA FOR 304 STAINLESS STEEL

FULLY SOFTENED AND ROLLED AT 300°C

TESTED IN MgCl$_2$ AT 140°C

% Reduction	0.5% Proof Stress (psi)	Applied Stress (psi)	Time to Failure (min)
0	32,770	40,000	71
0	32,770	40,000	77
6	56,000	40,000	690
10	67,510	40,000	390
10	67,510	40,000	384
18	81,000	40,000	330
27	89,200	40,000	322
27	89,200	40,000	318
10	67,510	75,000	10
10	67,510	75,000	7
18	81,000	75,000	114
27	89,200	75,000	144
27	89,200	75,000	168
44	100,000	75,000	168
44	100,000	75,000	283
50	103,060	75,000	144
50	103,060	75,000	168
50 *	Not determined	75,000	972

* Rolled at room temperature resulting in a duplex worked austenite + strain-induced martensite structure.

ARF 2152-18
(Final Report)

TABLE X

TIME-TO-FAILURE DATA FOR 304 STAINLESS STEEL

FURNACE COOLED FROM 982°C AND ROLLED AT 300°C

TESTED IN MgCl2 AT 140°C

% Reduction	0.5% Proof Stress (psi)	Applied Stress (psi)	Time to Failure (min)
0	21,900	40,000	144
0	21,900	40,000	126
7	50,000	40,000	6060*
27	84,300	40,000	5232
7	50,000	75,000	0.75^{+}
27	84,300	75,000	162
27	84,300	75,000	186
44	101,800	75,000	192
44	101,800	75,000	270

* Specimen did not fracture--no evidence of cracking on removal from test.

+ Ductile type failure--little evidence of stress-corrosion cracking on
removal from test.

TABLE XI

TIME-TO-FAILURE DATA FOR 304 STAINLESS STEEL

FULLY SOFTENED, ROLLED AT 300° C,

AND ANNEALED AT 700°C FOR 168 HOURS,

TESTED IN MgCl$_2$ AT 140°C

% Reduction	0.5% Proof Stress (psi)	Applied Stress (psi)	Time to Failure (min)
0	29,200	40,000	714
0	29,200	40,000	870
15	51,000	40,000	6888*
15	51,000	75,000	84
50	64,000	75,000	168
50	64,000	75,000	150

* Specimen did not fracture--no evidence of cracking on removal from test.

TABLE XII

TIME-TO-FAILURE DATA FOR 304 STAINLESS STEEL, FULLY SOFTENED AND ROLLED 15% AT DIFFERENT TEMPERATURES, TESTED IN $MgCl_2$ AT 140°C

Rolling Temperature (°C)	0.5% Proof Stress (psi)	Applied Stress (psi)	Applied Stress: UTS Ratio	Time to Failure (min)
23	54,286	40,000	--	408
23	54,286	75,000	0.83	162
-50	63,888	75,000	--	7212*
-50	63,888	102,000	0.83	366
-50	63,888	110,000	--	72
-196	79,096	40,000	--	7500*
-196	79,096	75,000	--	7500*
-196	79,096	110,000	--	6700
-196	79,096	127,000	0.83	3420

* Specimen did not fracture - no evidence of cracking on removal from test.

ARMOUR RESEARCH FOUNDATION OF ILLINOIS INSTITUTE OF TECHNOLOGY

ARF 2152-18
(Final Report)
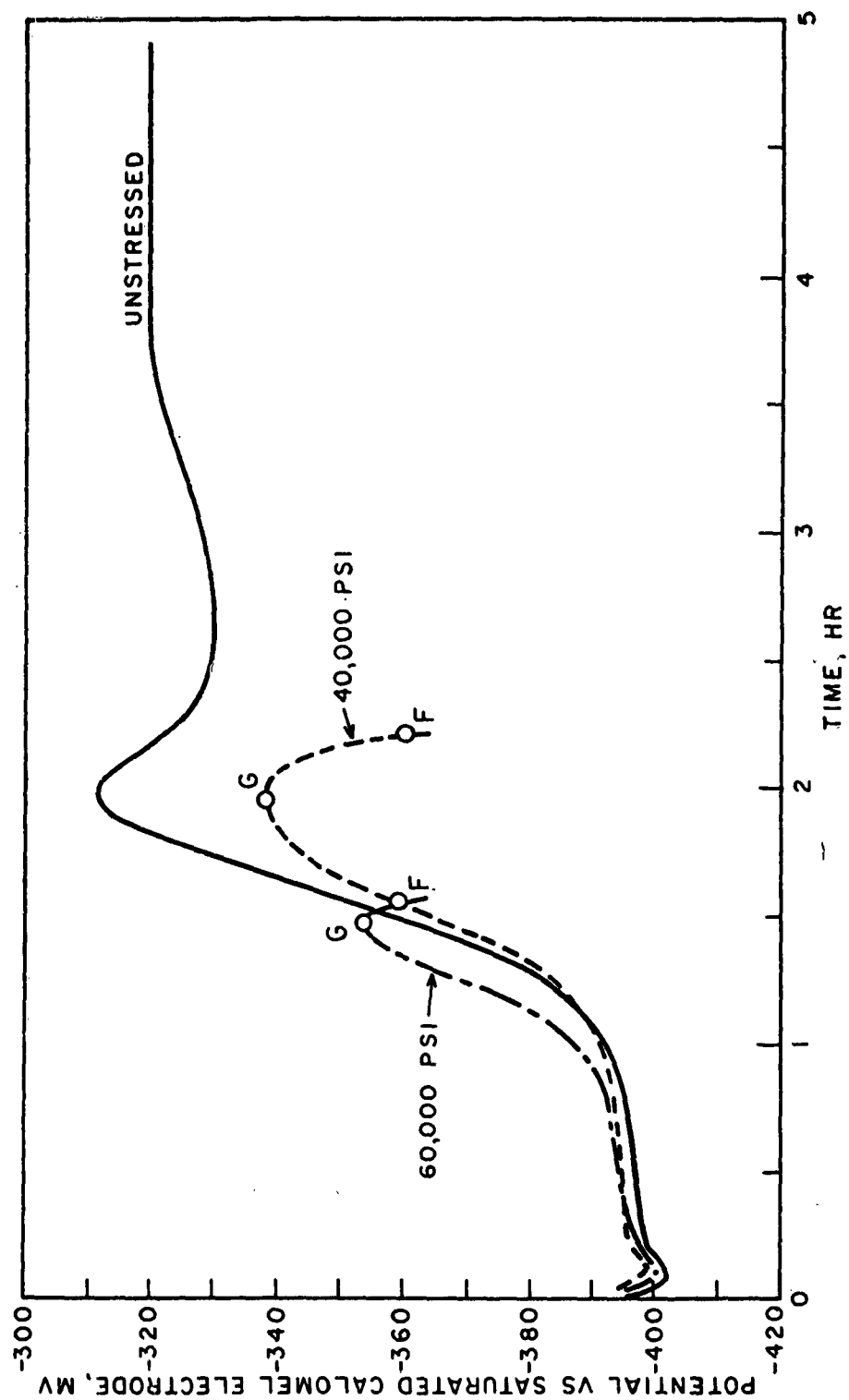
Figure 1 - Effect of Stress on Corrosion of 18-8 Stainless Steel in 42% MgCl₂ at 146°C. (After Barnartt & van Rooyen,(3) - modified to include an initial fall at the beginning of each curve).
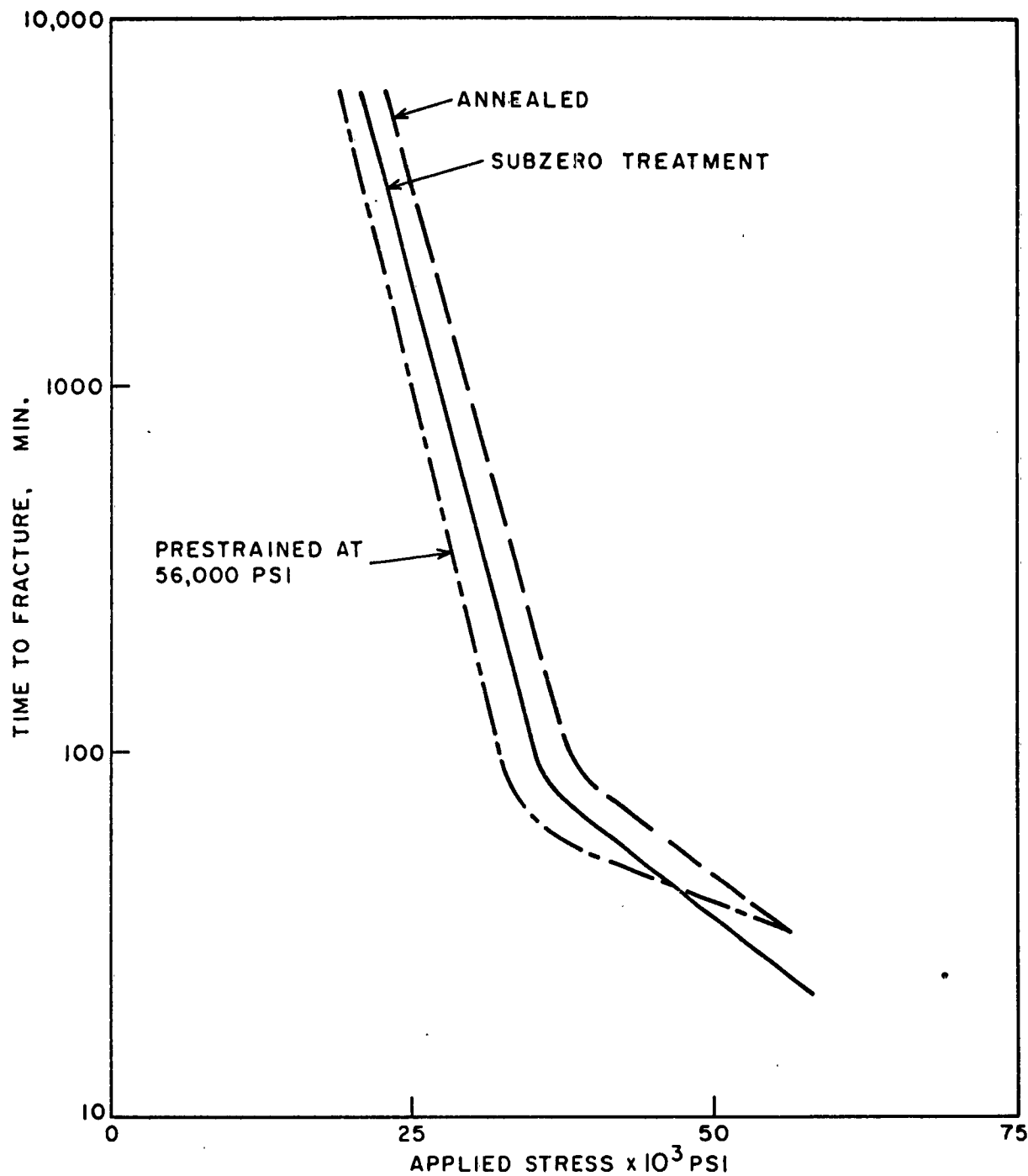
Figure 2 - Variation of Time to Fracture With Applied Stress.
Steel 18-8: Fully Softened; Prestrained at 56,000
lb/in^2; And Refrigerated at -184°C For 1/2 Hr.
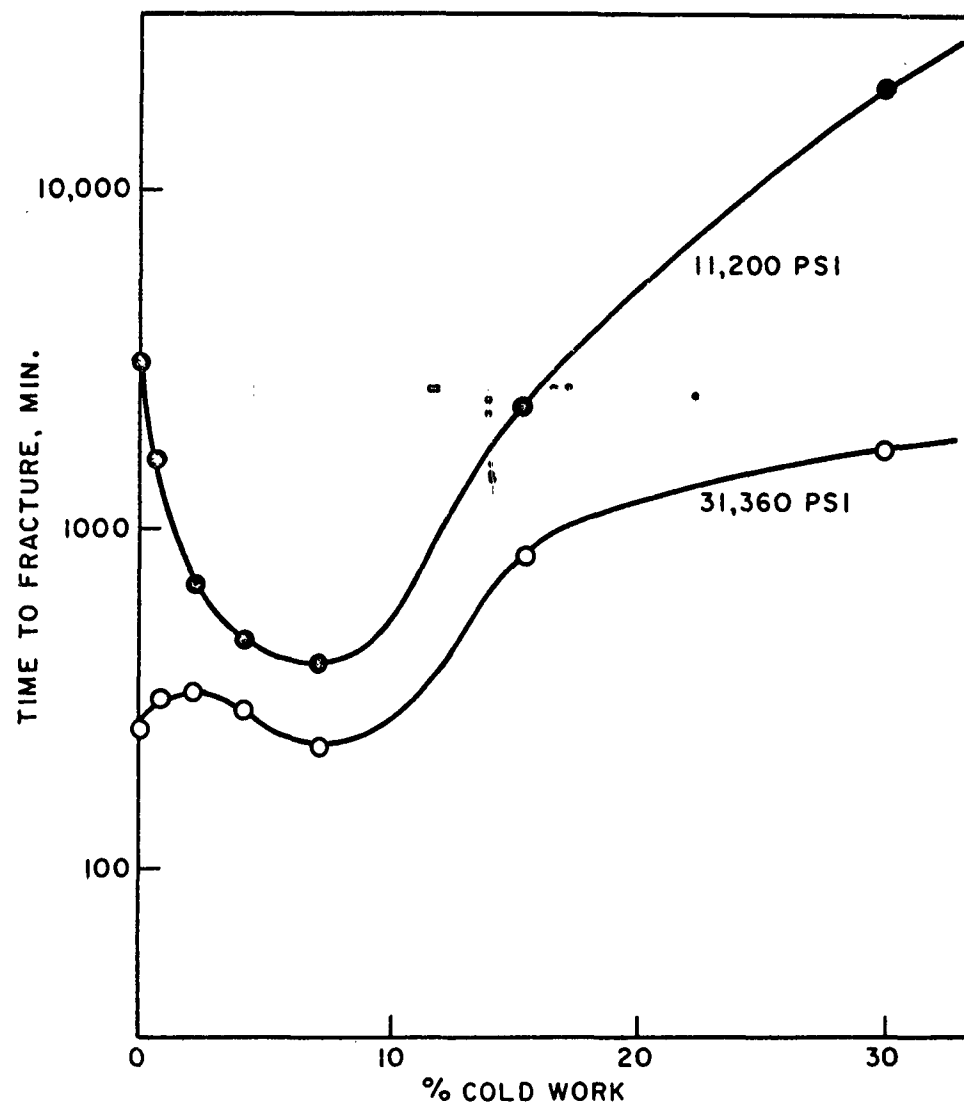Tested at 152-153°C. (Hoar & Hines[5])

ARF 2152-18
                                (Final Report)

Figure 3 - Variation of Time to Fracture With Amount
Of Previous Cold Working for Specimens Of
An 18-8 Ti Steel Tested In Boiling 42% $MgCl_2$
Solution. (Hines[14])
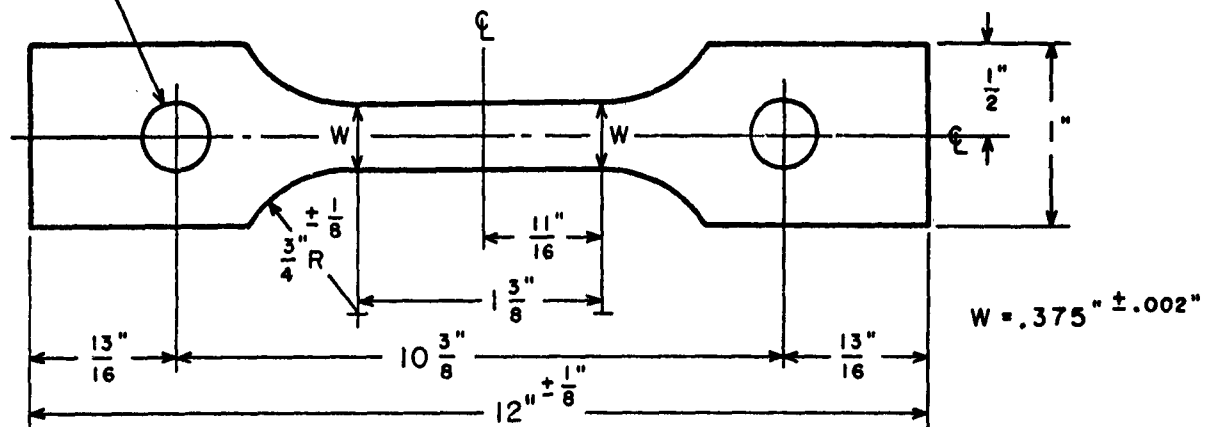
Figure 4 - Dimensions of the Strip Stress-Corrosion Test Specimens.
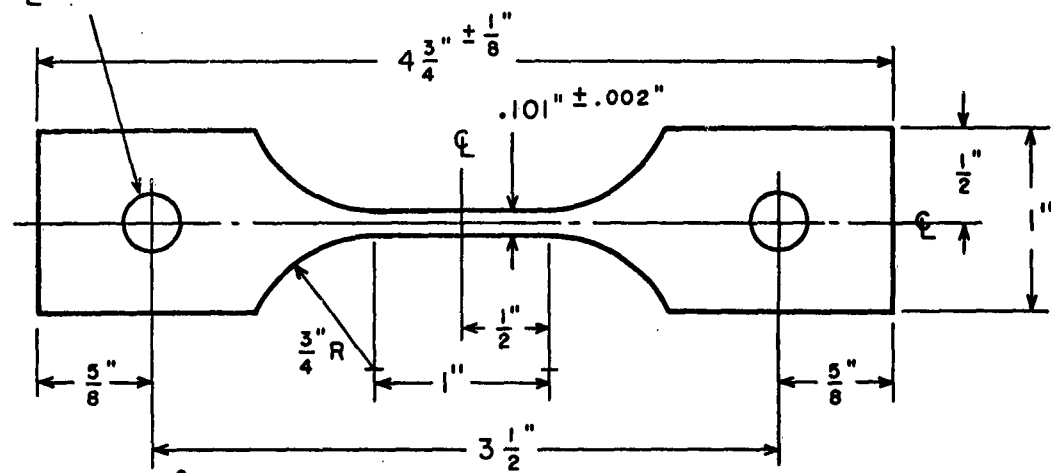
Figure 5 - Dimensions of the Strip Tensile Test Specimens.
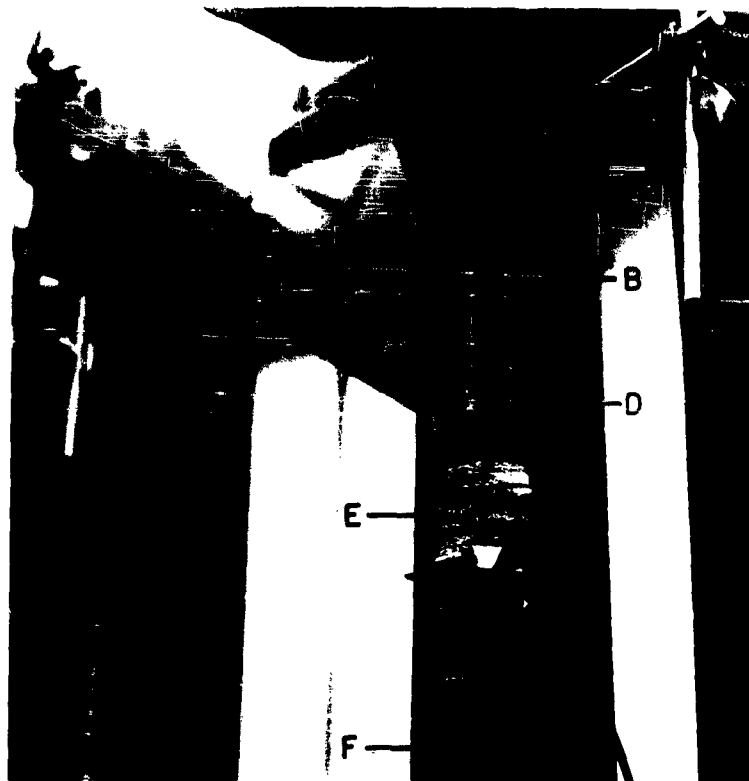
Neg. No. B-546

Figure 6

Assembly for Testing Specimens in $MgCl_2$ at 140°C
Under Tensile Loading.

A - Dial Gage Indicating Specimen Extension
B - Controller Thermocouple
C - Thermometer
D - Top Part of Specimen
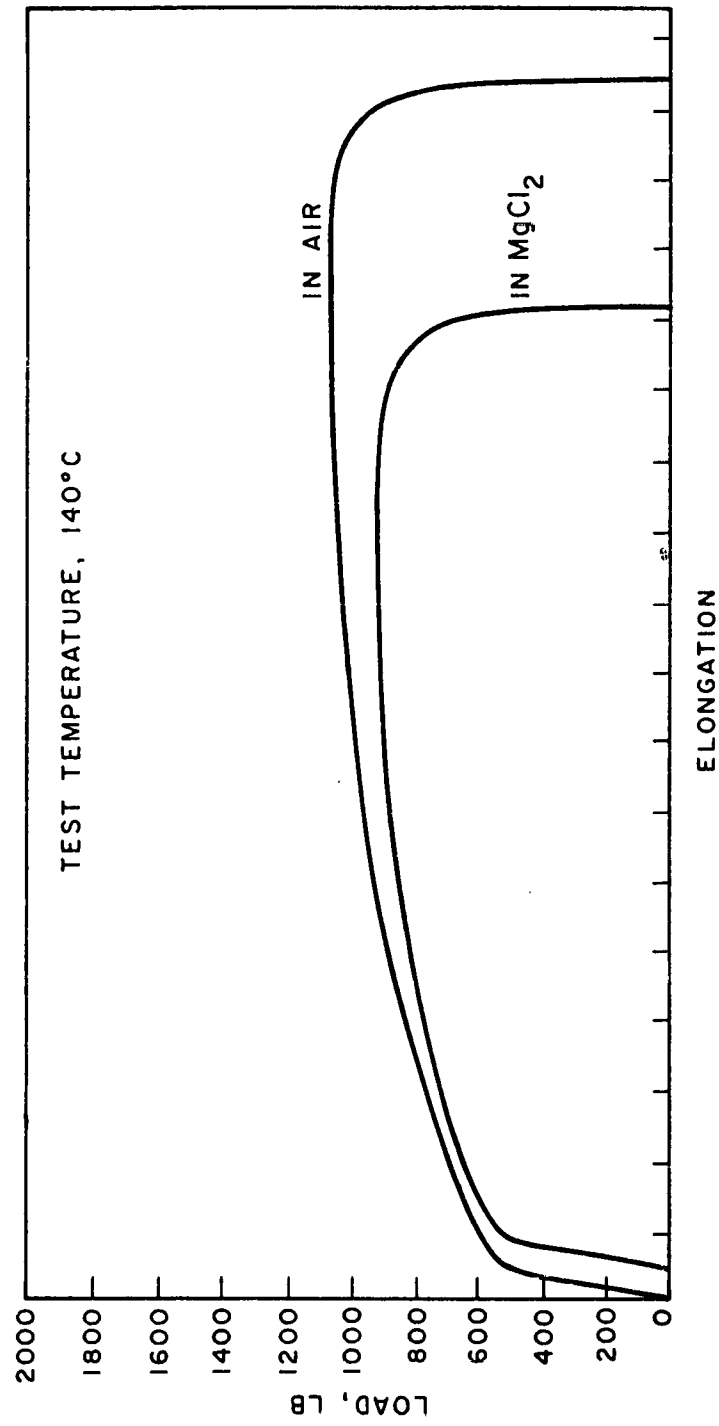E - Test Cell Wrapped with Heating Element
F - Creep Stand

Figure 7 - Load-Elongation Curves for 304 Stainless Steel Tested in Air and MgCl₂.

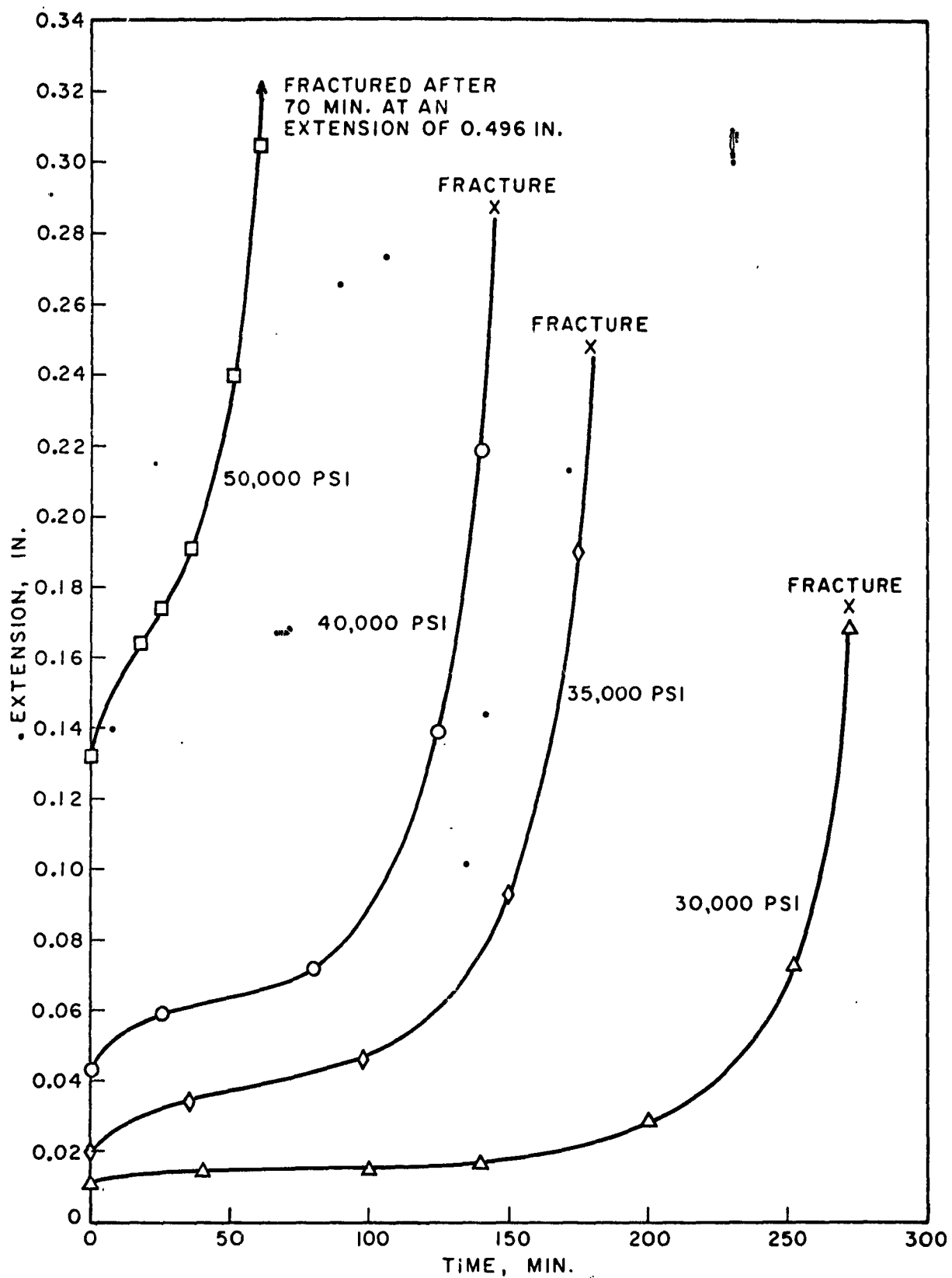ARF 2152-18
(Final Report)

Figure 8 - Extension-Time Data for 304 Stainless Steel Tested
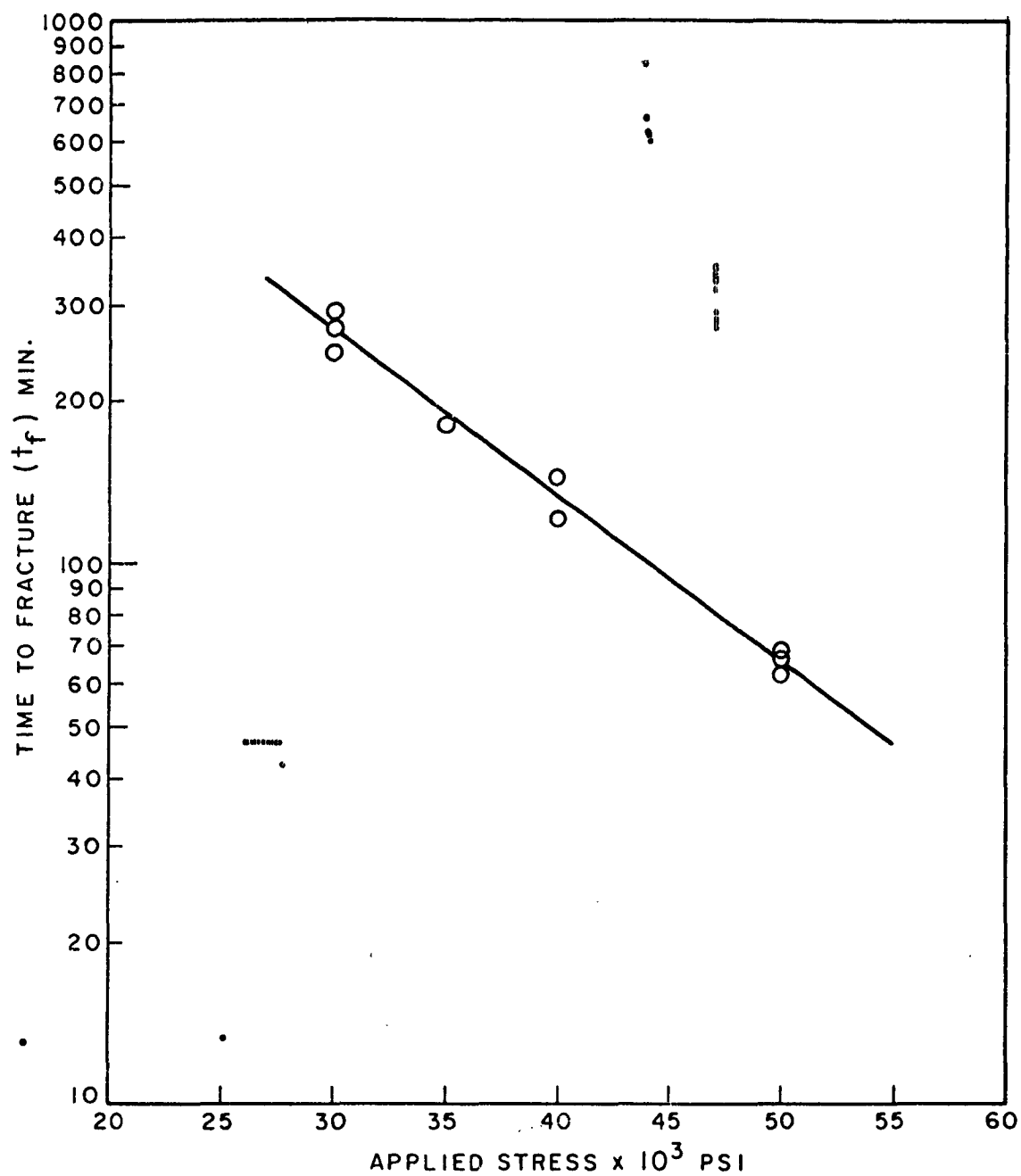In MgCl$_2$ at 140°C.

Figure 9 - Relationship Between Applied Stress and Time to Failure
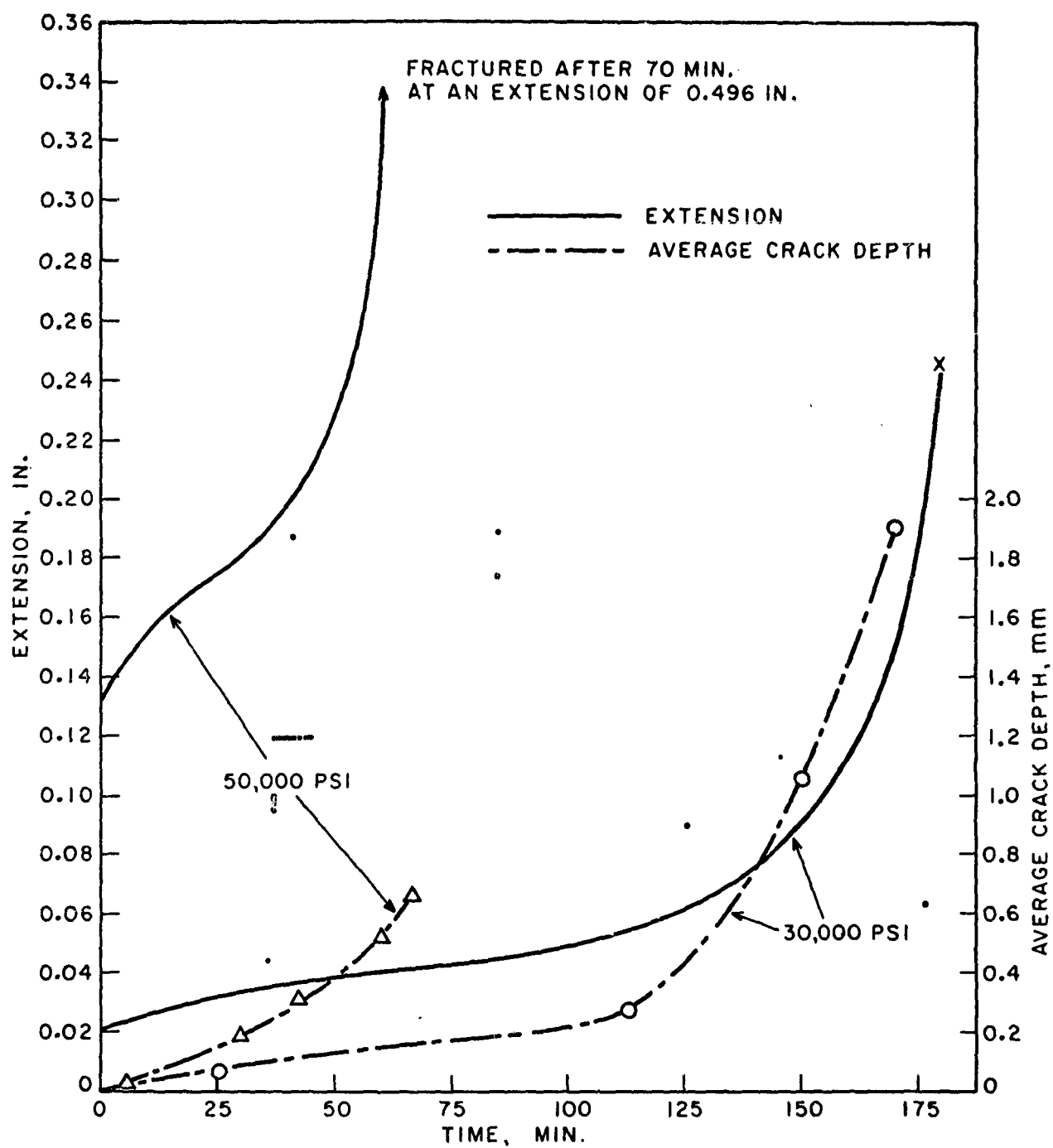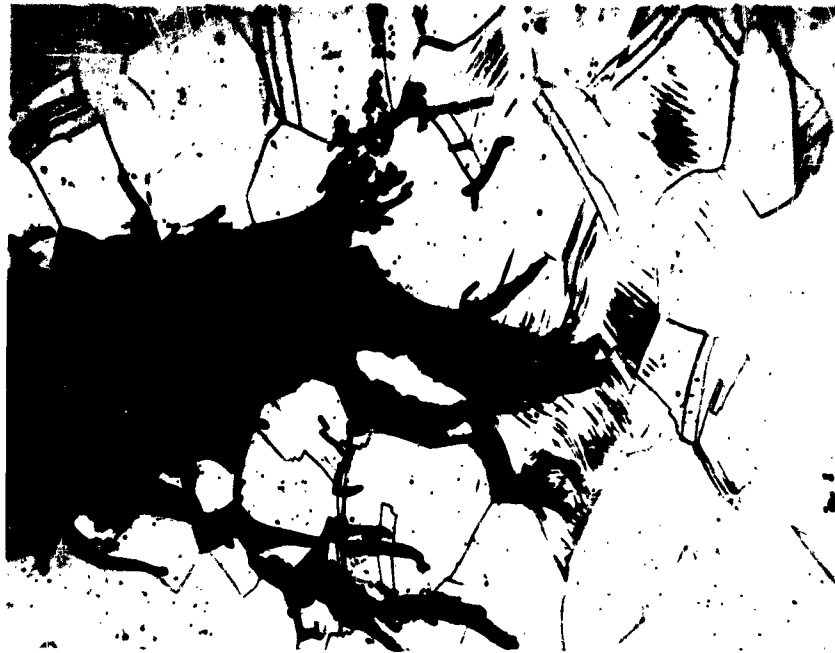For 304 Stainless Steel Tested in $MgCl_2$ at 140°C.

Figure 10 - Crack Growth - Time and Extension - Time Data For 304
Stainless Steel Tested in MgCl$_2$ at 140°C.

ARF 2152-18
                                                      (Final Report)
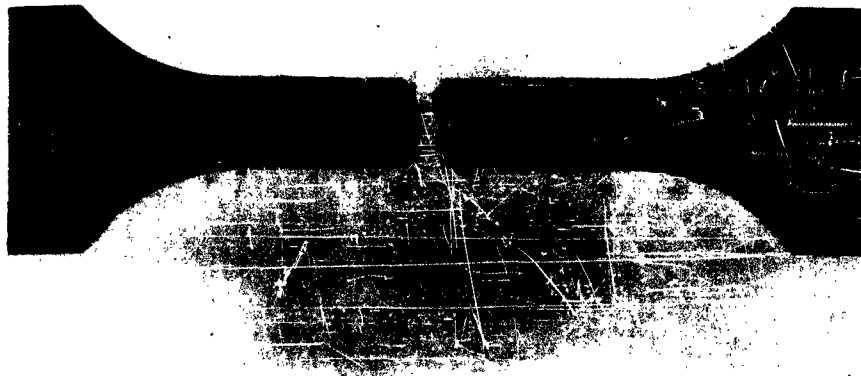
Neg. No. 21838   X250

Figure 11

Stress-corrosion cracks in fully softened
304 stainless steel tested in $MgCl_2$ at
140° C at an applied stress of 50, 000 psi.
(Etched)

Neg. No. 21354   X1.3

Figure 12

Crack pattern on a tensile specimen exposed
to $MgCl_2$ at 140°C at an applied stress of
30, 000 psi.

ARF 2152-18
                                     (Final Report)

Neg. No. 21356   X 1.3

Figure 13

Crack pattern on a tensile specimen exposed to $MgCl_2$ at 140°C at an applied stress of 40,000 psi.

Neg. No. 21355   X 1.3

Figure 14

Crack pattern on a tensile specimen exposed to $MgCl_2$ at 140°C at an applied stress of 50,000 psi.

Neg. No. 21357   X 1. 3

Figure 15

Crack pattern on a tensile specimen held in $MgCl_2$ at 140°C for
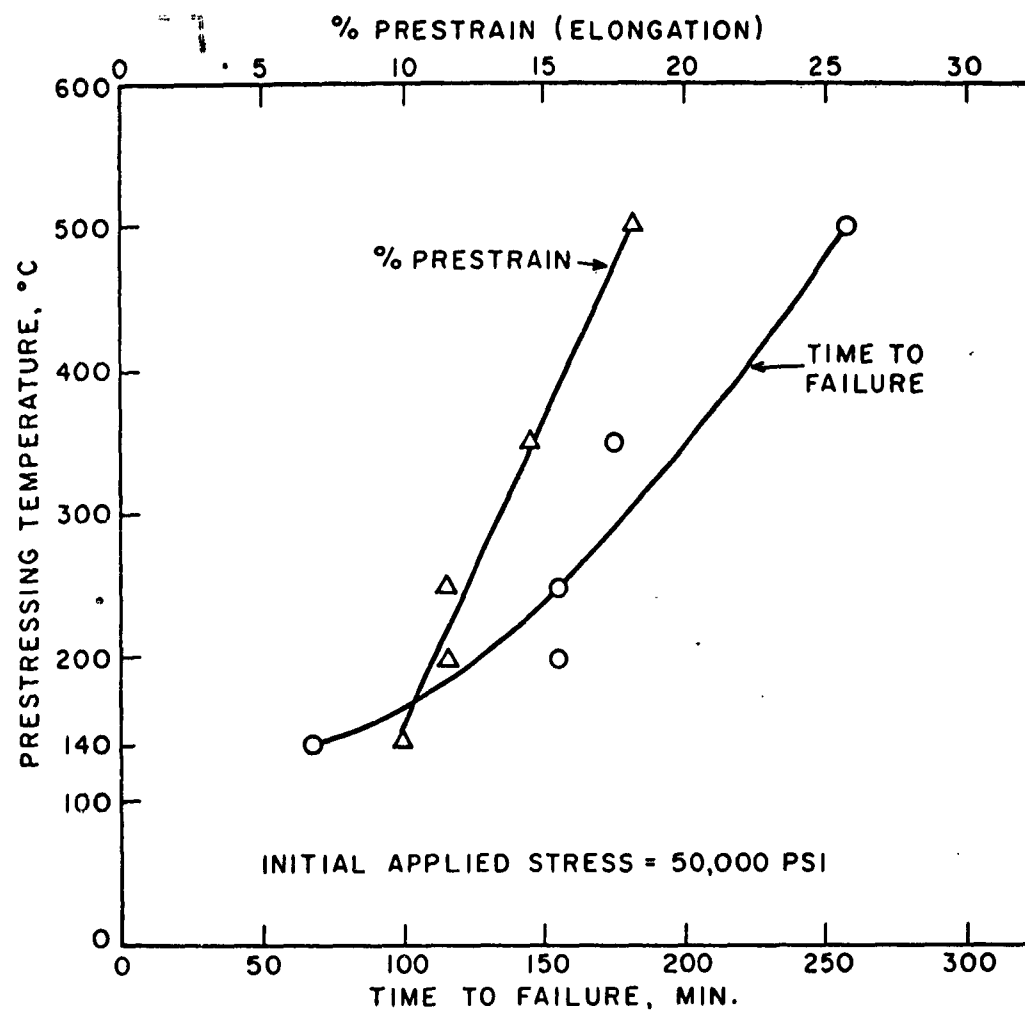960 min, then subjected to an applied stress of 50,000 psi to
fracture.

ARF 2152-18
(Final Report)

Figure 16 - Influence of Prestressing Temperature on Elongation
And Time To Failure For 304 Stainless Steel Tested
In $MgCl_2$ at 140°C.

Neg. No. 21851   X1.3

Figure 17

Crack pattern on a tensile specimen prestressed at
50,000 psi in air at 500°C and subsequently tested to
failure in $MgCl_2$ at 140° C.
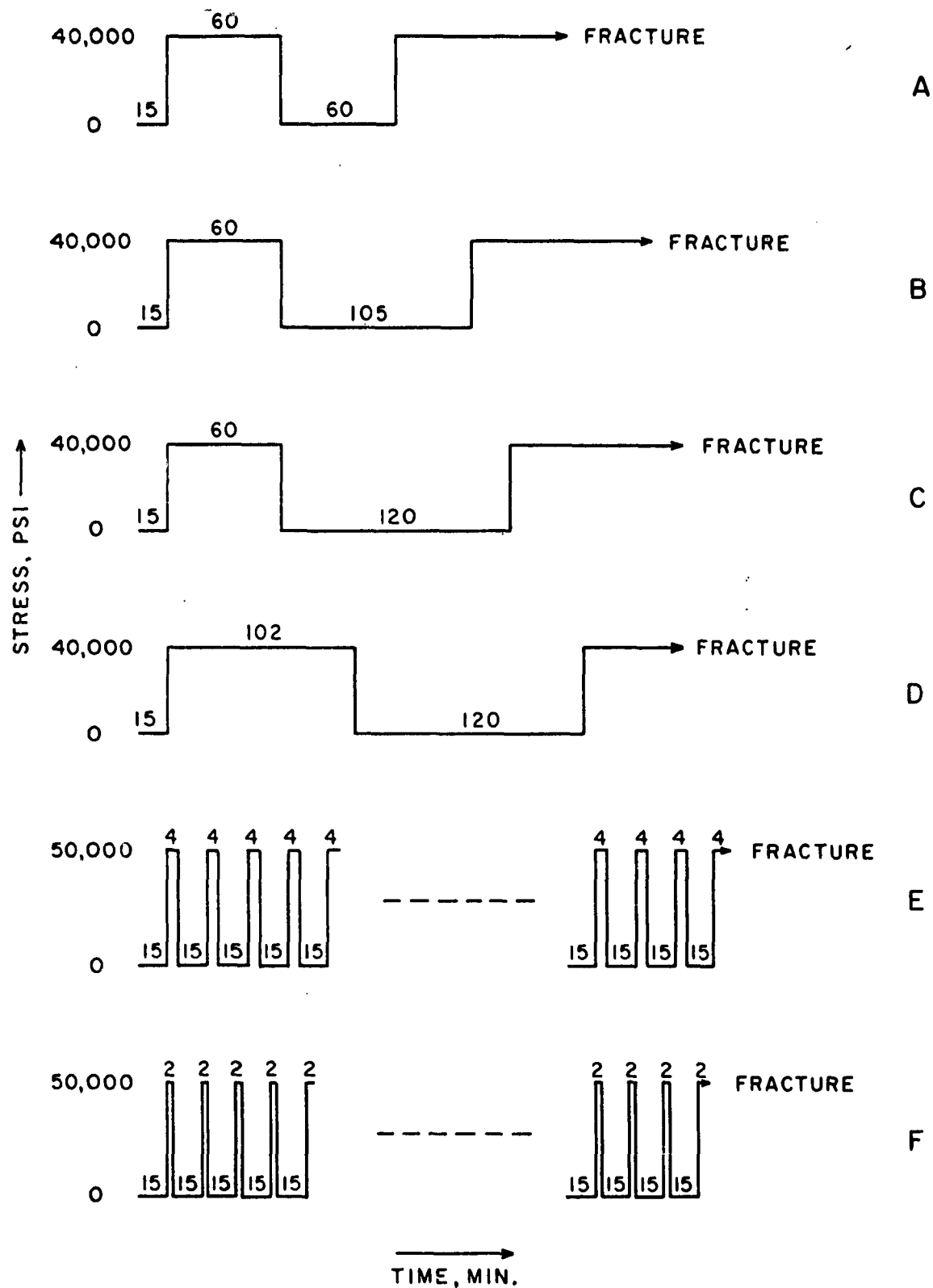
ARF 2152-18
(Final Report)

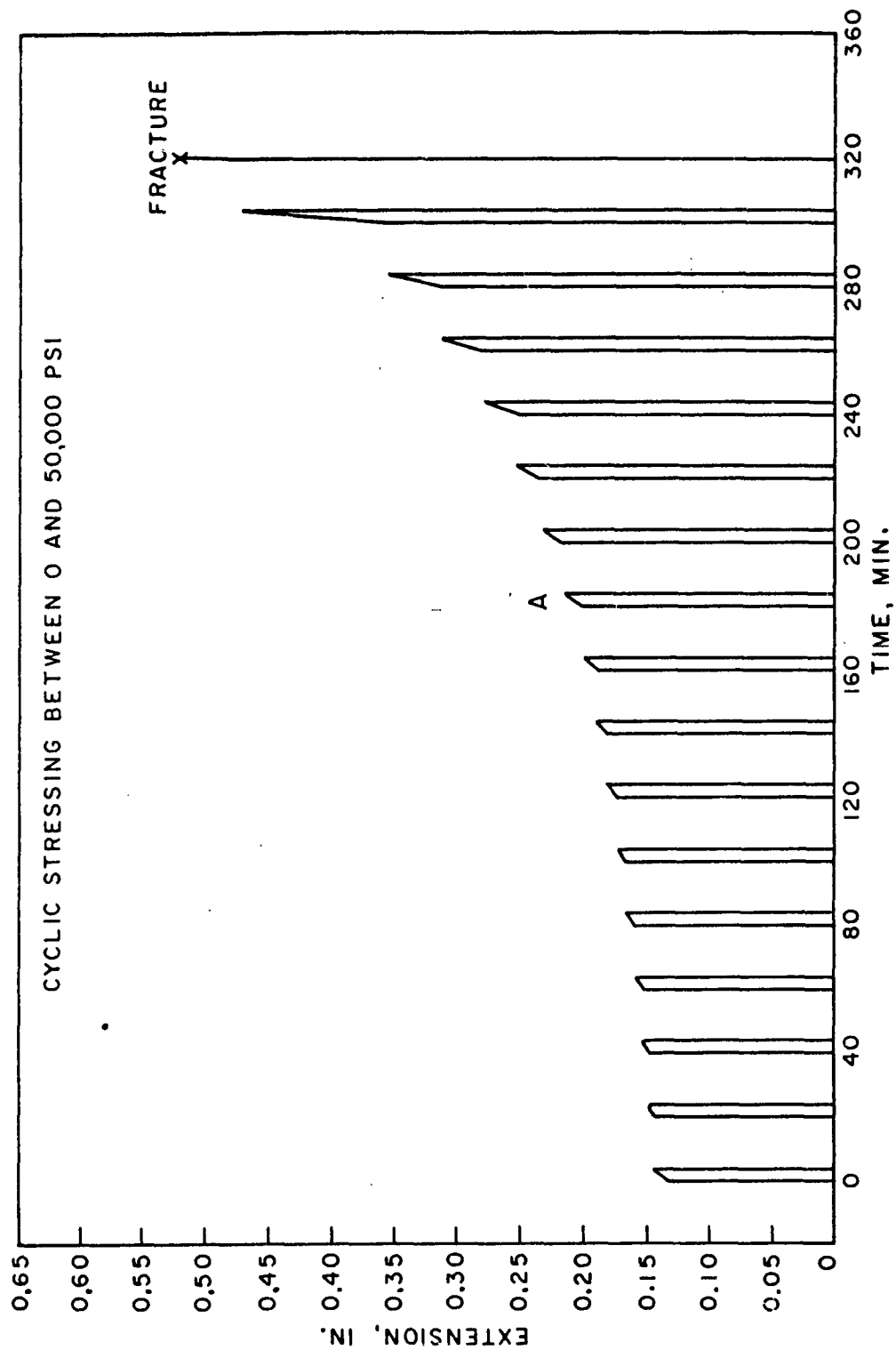Figure 18 - Schematic Representation of the Cycling Treatments.

Figure 19 - Extension-Time Curve for 304 Stainless Steel Tested in $MgCl_2$ at 140°C Under Cyclic Loading - 4 min at 50,000 psi, 15 min at 0 psi.
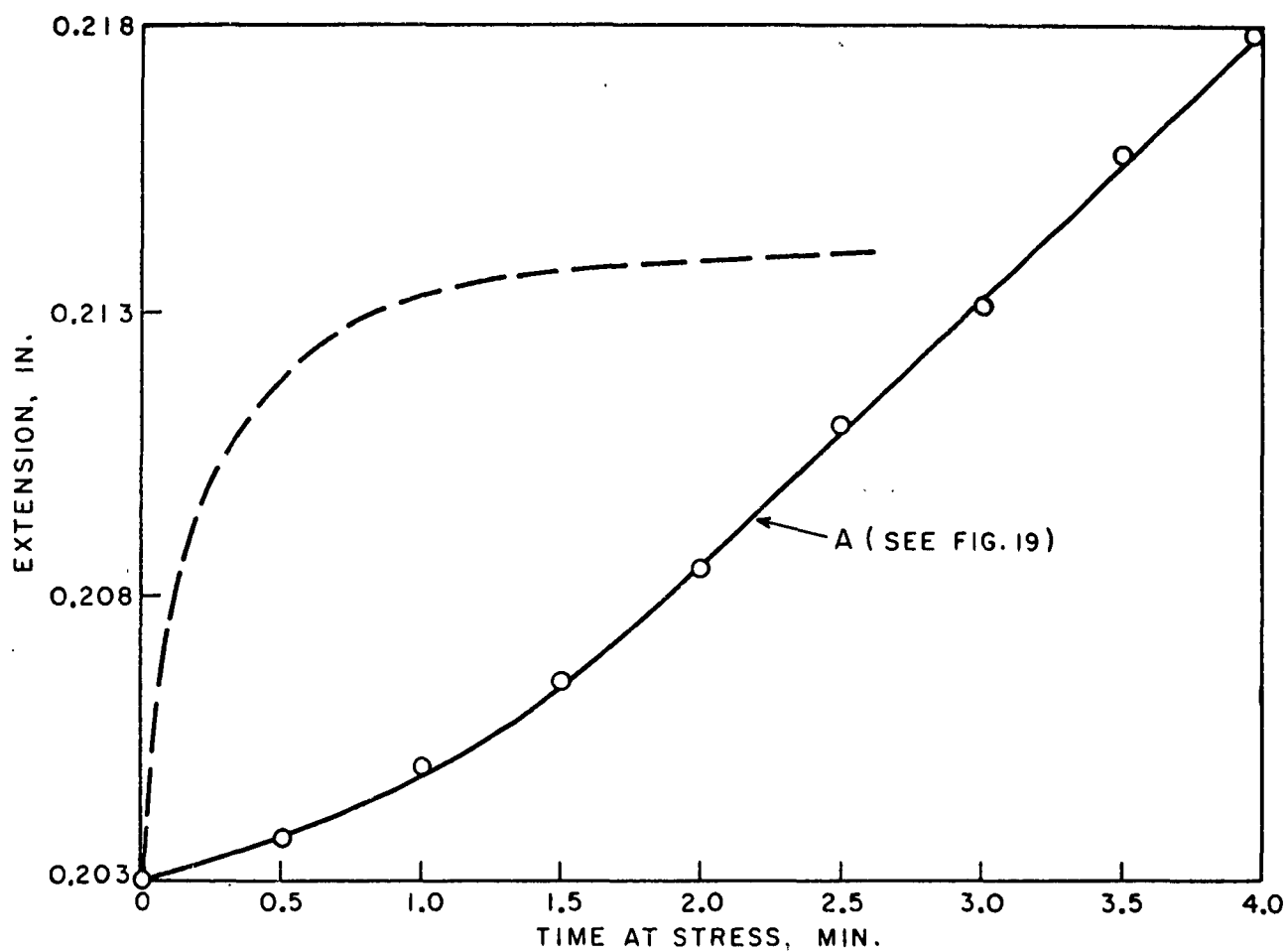
Figure 20 - Time Curve for 304 Stainless Steel Tested in $MgCl_2$ at 140°C. Curve Represents Peak A in Figure 19.
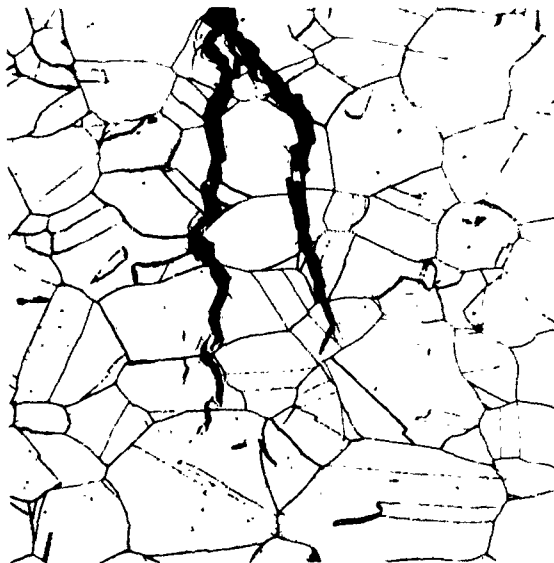
Neg. No. 21675   X250

Figure 21

Structure of 304 stainless steel rolled
15% at -196°C. The austenite has almost
completely transformed to strain-induced
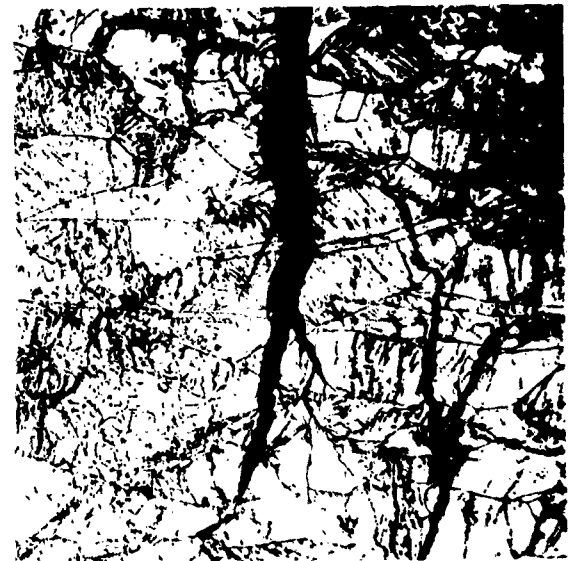martensite. Treatment (D).   (Etched)

Neg. No. 21787   X250

Figure 22

Stress-corrosion cracks in 304
stainless steel WQ from 982°C and
aged at 700°C for 168 hours. Tested
in MgCl2 at 140°C under an applied
stress of 40,000 psi. (Etched.

Neg. No. 21789   X250

Figure 23

Stress corrosion cracks in 304
stainless steel WQ from 982°C,
rolled 50% at 300°C, and aged at
700°C for 168 hours. Tested in
MgCl2 at 140°C under an applied
stress of 75,000 psi. (Etched)

- 67 -

Neg. No. 21673 •   X250

Figure 24

Stress-corrosion cracks in 304 stainless
steel furnace cooled from 982° C and tested
in $MgCl_2$ at 140° C under an applied stress
of 40,000 psi. (Etched)

Neg. No. 21837   X250

Figure 25

Transgranular and intergranular cracks in
304 stainless steel WQ from 982° C and
rolled 27% at 300 °C. Tested in $MgCl_2$ at
140° C under an applied stress of 75,000 psi.
(Etched)

- 68 -•
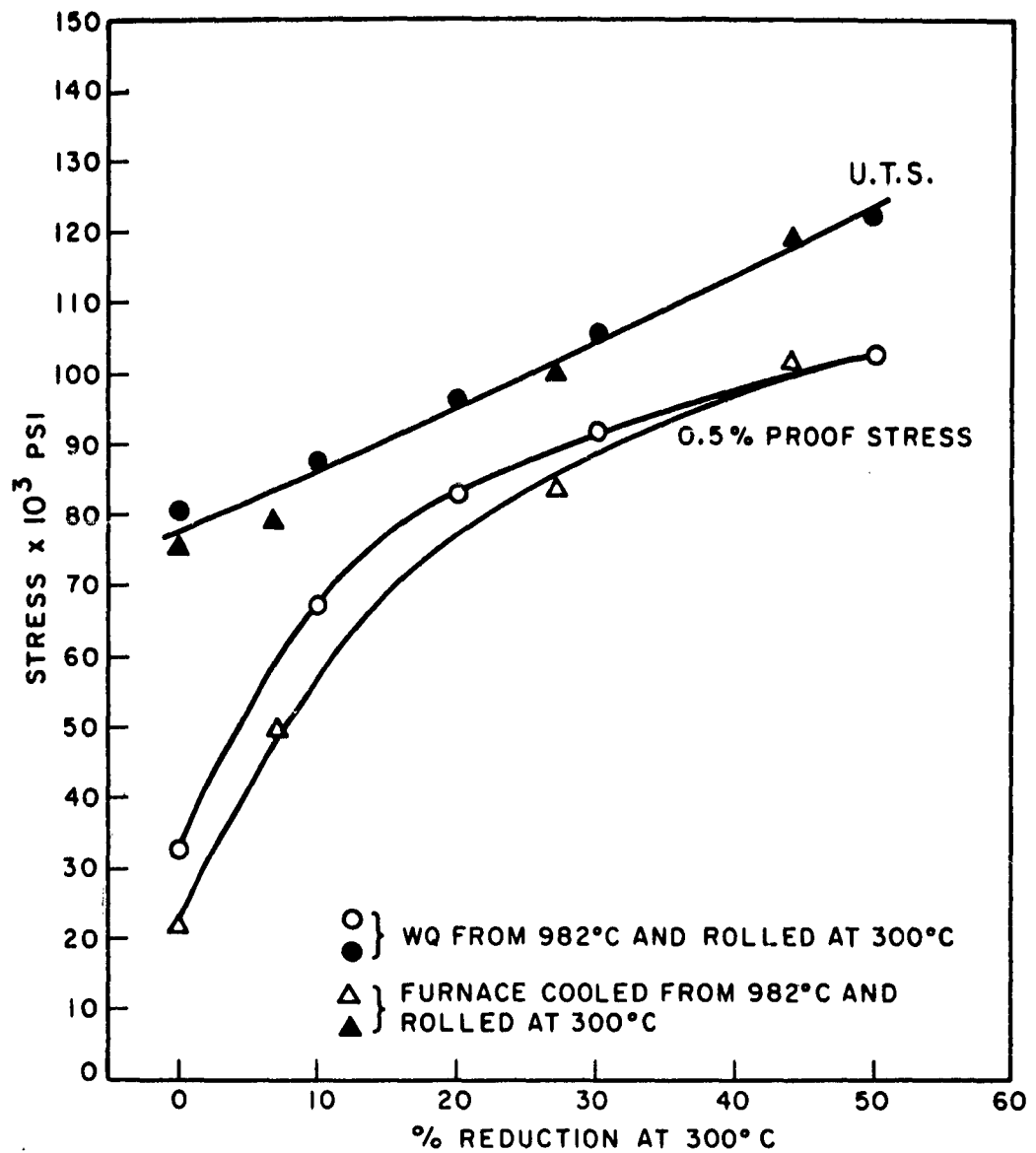
Figure 26 - Variation of Tensile Properties With % Reduction
At 300°C.

ARF 2152-18
(Final Report)
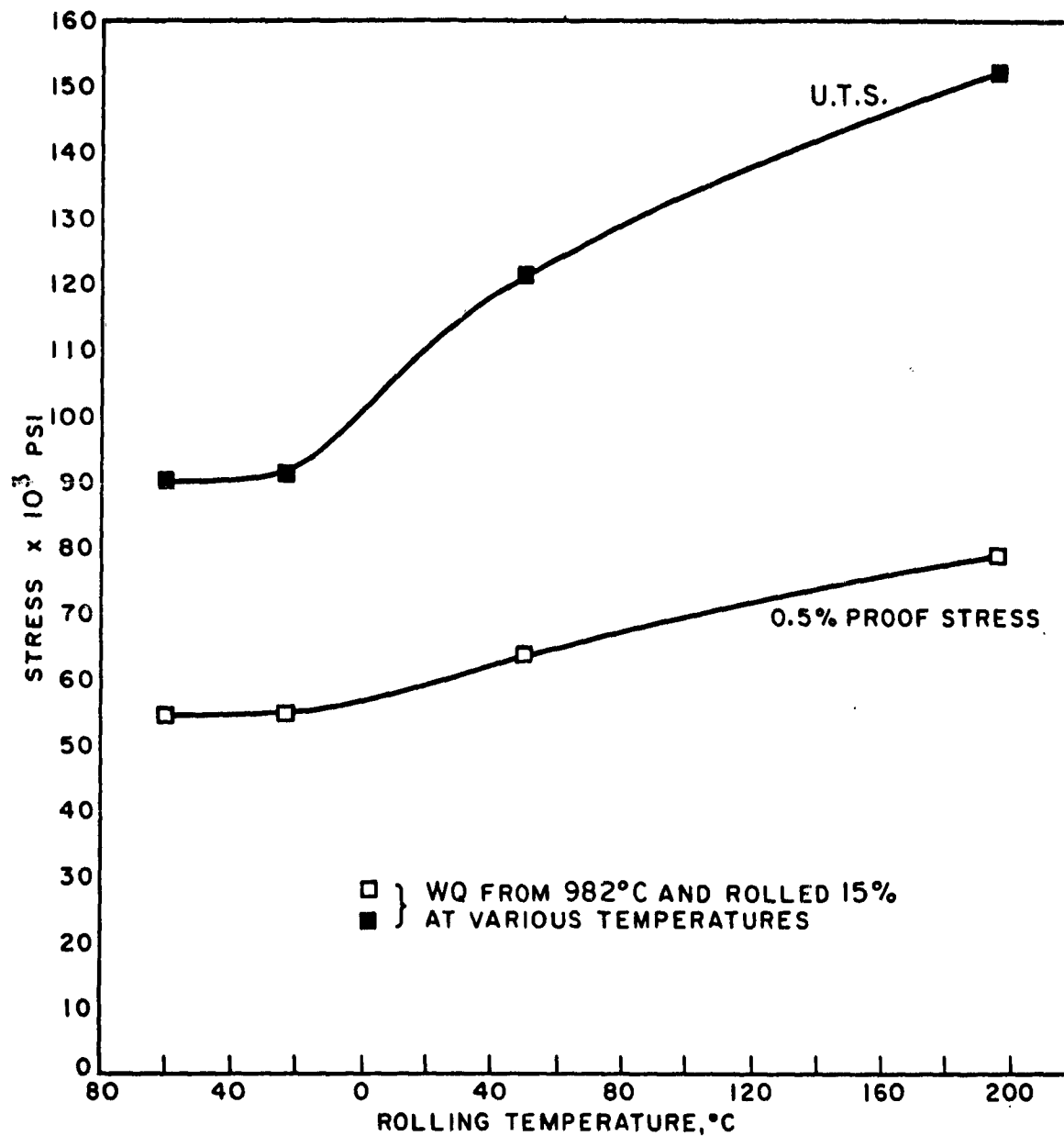
Figure 27 - Variation of Tensile Properties With Rolling Temperature.

ARF 2152-18
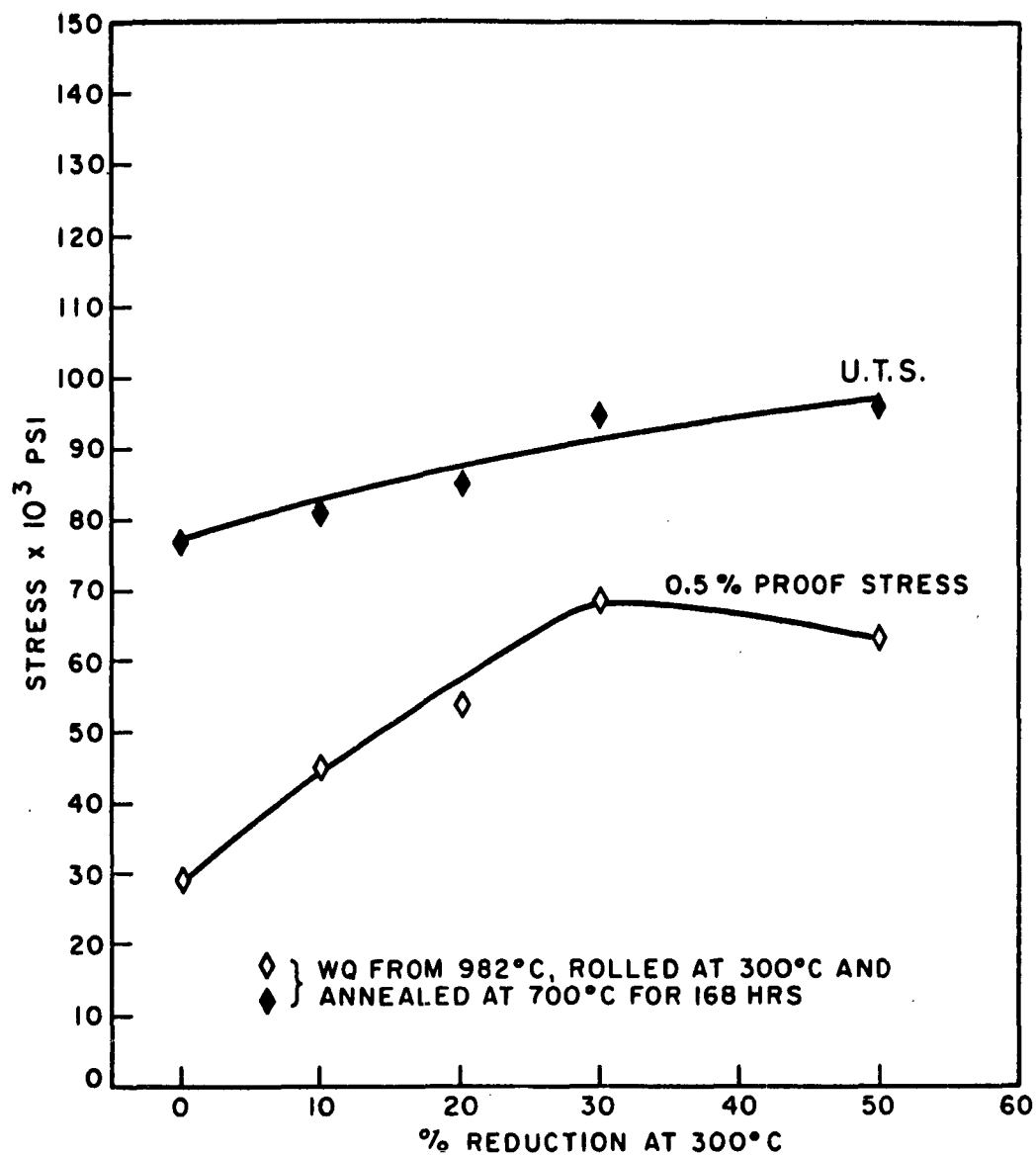(Final Report)

Figure 28 - Variation of Tensile Properties After Rolling At
300°C & Annealing at 700°C For 168 Hours.
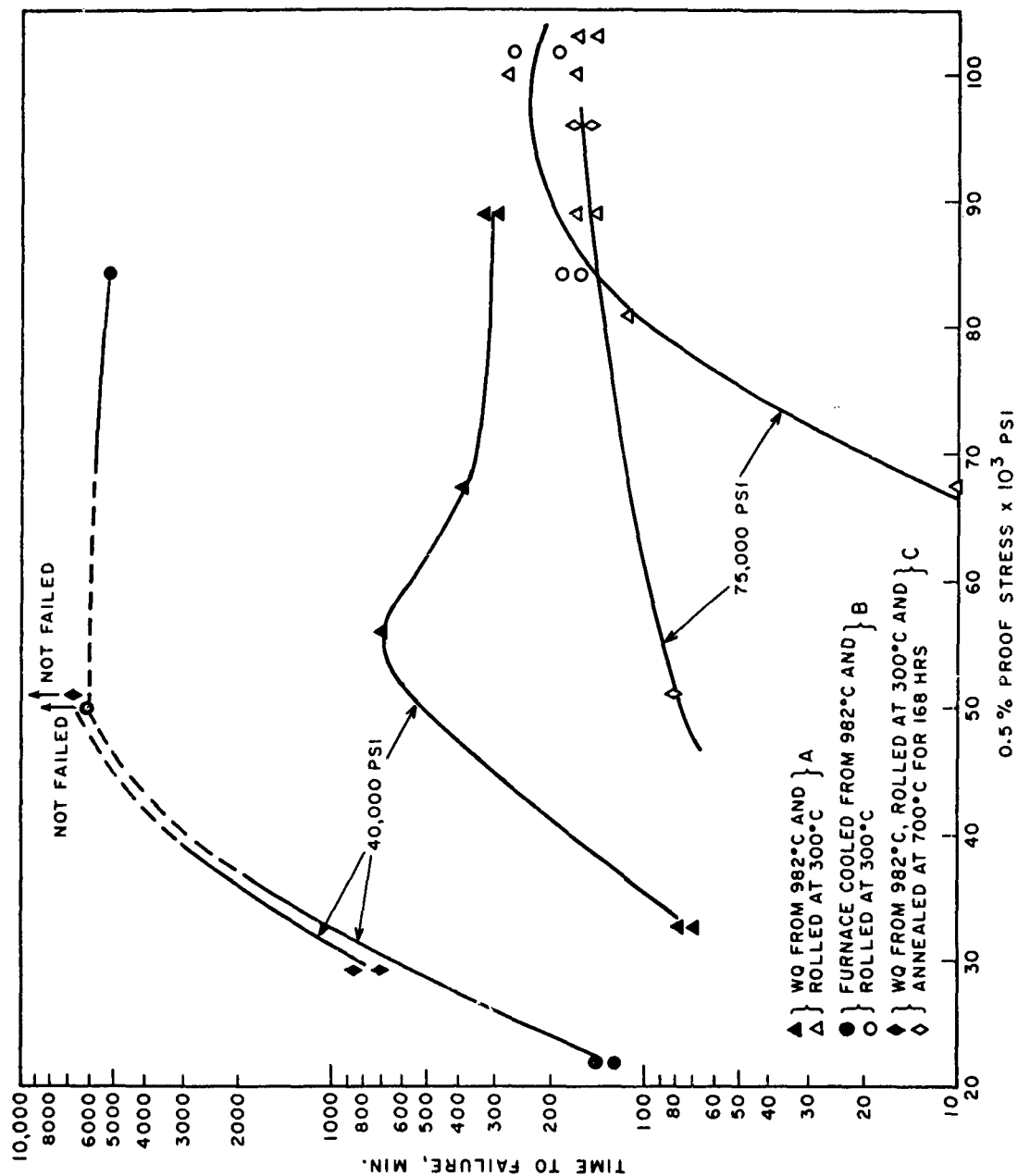
Figure 29 - Time to Failure - 0.5% Proof Stress Data for Treatments (A) (B) and (C).
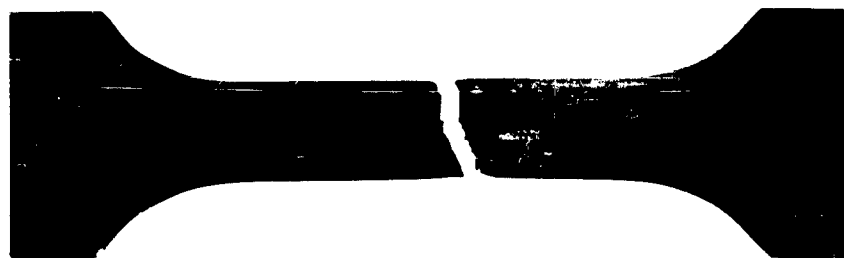
Neg. No. 21679   X 1.3

Figure 30

Crack pattern on a tensile specimen rolled 27% at 300°C
and tested in $MgCl_2$ at 140°C at a stress of 75,000 psi.

Neg. No. 21742   X500

Figure 31

Fracture surface structure of fully softened
304 stainless steel showing irregular fracture
pattern.

Neg. No. 21739   X500

Figure 32

Chevron type fracture pattern observed in
fully softened 304 stainless steel and taken
from the same specimen as in Figure 31.
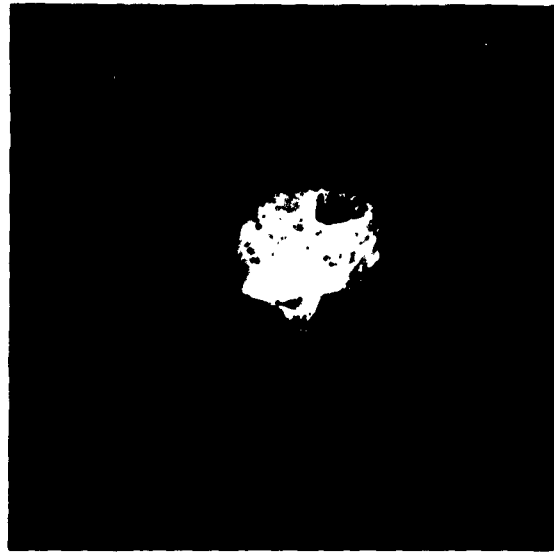
Neg. No. 21741   X500

Figure 33

Fracture surface structure of fully softened
304 stainless steel showing cleavage type
fracture.

Neg. No. 21736   X500

Figure 34

Fracture surface structure of 304 stainless
steel rolled 15% at -196°C prior to testing.
Illustrates typical cleavage type fracture.

ARF 2152-18
                                 (Final Report)

APPENDIX

SUMMARY OF EXPERIMENTAL WORK
CARRIED OUT BETWEEN JUNE 15, 1958, AND JULY 31, 1960.[*]

This appendix contains a brief summary of the work carried out during the first two years on Contract No. Nonr-2602(00). The objective of the experimental work was to analyze the specific behavior characteristics of stress-corrosion embrittlement with the hope that this phenomenon could be brought within the present concepts of brittle fracture. Particular attention was paid to the role of surface energy, a parameter fundamental to all current theories of fracture.

Theoretical Discussion

The phenomenon of fracture of a metal under static load in the presence of some particular liquid or gaseous medium is known as stress-corrosion embrittlement. This has been interpreted classically to originate as a corrosion phenomenon, hence, the name.

In the last several years, principally by Stroh and Petch, theories have been developed to correlate brittle fracture with dislocation theory. Essentially, these models postulate the formation of a crack nucleus by the coalescence of dislocations in existence or produced by deformation processes. It has been shown theoretically and experimentally that the relationship between fracture stress and grain size in brittle fracture is of the form:

[*] For a detailed account of this work, see reports ARF 2152-7 and ARF 2152-13.

ARMOUR RESEARCH FOUNDATION OF ILLINOIS INSTITUTE OF TECHNOLOGY

ARF 2152-18
(Final Report)

$$\sigma_f = \sigma_o + k \left(\frac{1}{d} \right)^{1/2} \tag{A-1}$$

where σ_f = fracture stress

d = average grain diameter

σ_o and k are constants.

Petch proposed a model of hydrogen embrittlement of mild steel which correlated embrittlement and reduction in surface energy, γ, with adsorbed hydrogen on the crack nucleus. He proposed that equation (A-1) be modified to:

$$\sigma_f = \sigma_o + 4 \left[\frac{3 \mu \gamma}{\pi (1-\nu)} \right]^{1/2} \cdot \left[\frac{1}{d} \right]^{1/2} \tag{A-2}$$

in which γ = surface energy of the crack

μ = modulus of rigidity

ν = Poisson's ratio

Thus, from the slope of the fracture stress-grain diameter it is possible to calculate the surface energy. Petch demonstrated that the surface energy of iron was reduced by hydrogen from 1600 to about 650 ergs/cm^2.

That equation (A-2) is correct has been demonstrated by Stroh[13] by the fact that surface energies calculated for iron, zinc, magnesium, and molybdenum are in good agreement with those derived by other methods.

The above approach was used in a study of the stress-corrosion cracking phenomenon. Specimens of a variety of susceptible materials

ARMOUR RESEARCH FOUNDATION OF ILLINOIS INSTITUTE OF TECHNOLOGY

ARF 2152-18
(Final Report)

covering a range of grain sizes were prepared and tested in uniaxial tension under conditions of continuous loading in an environment known to produce stress-corrosion cracking. Some tests were also performed in air.

Preliminary experiments in which specimens were rapidly loaded to arbitrary stress levels, unloaded, and examined demonstrated that cracking did occur at critical and reproducible stress levels. It was concluded that the initiation of brittle fracture can be achieved in a stress-corrosion medium by continuous loading in tension. The stress level required to produce the first visible signs of cracking at X20 magnification was taken as the brittle fracture stress (σ_f) for that particular grain size (d). A series of specimens covering a range of grain sizes was tested in this way in order to determine the σ_f-$d^{-1/2}$ relationship given in equation A-1. The constant k was then determined from a graphical plot of these two parameters and, with μ and ν known, the surface energy associated with fracture was calculated.

Results

The results obtained in this phase of the program are summarized in Table A-I and Figures A-1 to A-4 . Limitation of experimental funds did not permit the determination of the surface energy for Al-4 Cu and Armco iron to be made under non-stress corrosion conditions.

Conclusions

The onset of embrittlement under stress-corrosion conditions in 304 stainless steel Mg-6Al, Al-4Cu, and Armco iron has been analyzed in terms of the Petch equation relating fracture stress (σ_f) and grain size (d).

ARMOUR RESEARCH FOUNDATION OF ILLINOIS INSTITUTE OF TECHNOLOGY

ARF 2152-18
(Final Report)

In all cases a linear relationship between σ_f and $d^{-1/2}$ was observed and thus permitted the calculation of surface energies from the slopes of the respective curves.

The data for 304 stainless steel and Mg-6Al clearly indicate the effectiveness of a stress-corrosion medium in lowering the surface energy associated with fracture. Although surface energies for Al-4Cu and Armco iron were not de.crmined in a non-stress corroding medium, the extremely low values determined under stress-corrosion conditions strongly suggest that, here again, there was a reduction in surface energy.

It was suggested that the lowering of surface energy might have been due to the adsorption of critical ion species generated by electrochemical processes, at crack sites. The results certainly make a valuable contribution to the development of a dislocation-surface energy model to account for the stress-corrosion cracking phenomenon.

TABLE A-1

SUMMARIZED DATA ON SURFACE ENERGIES

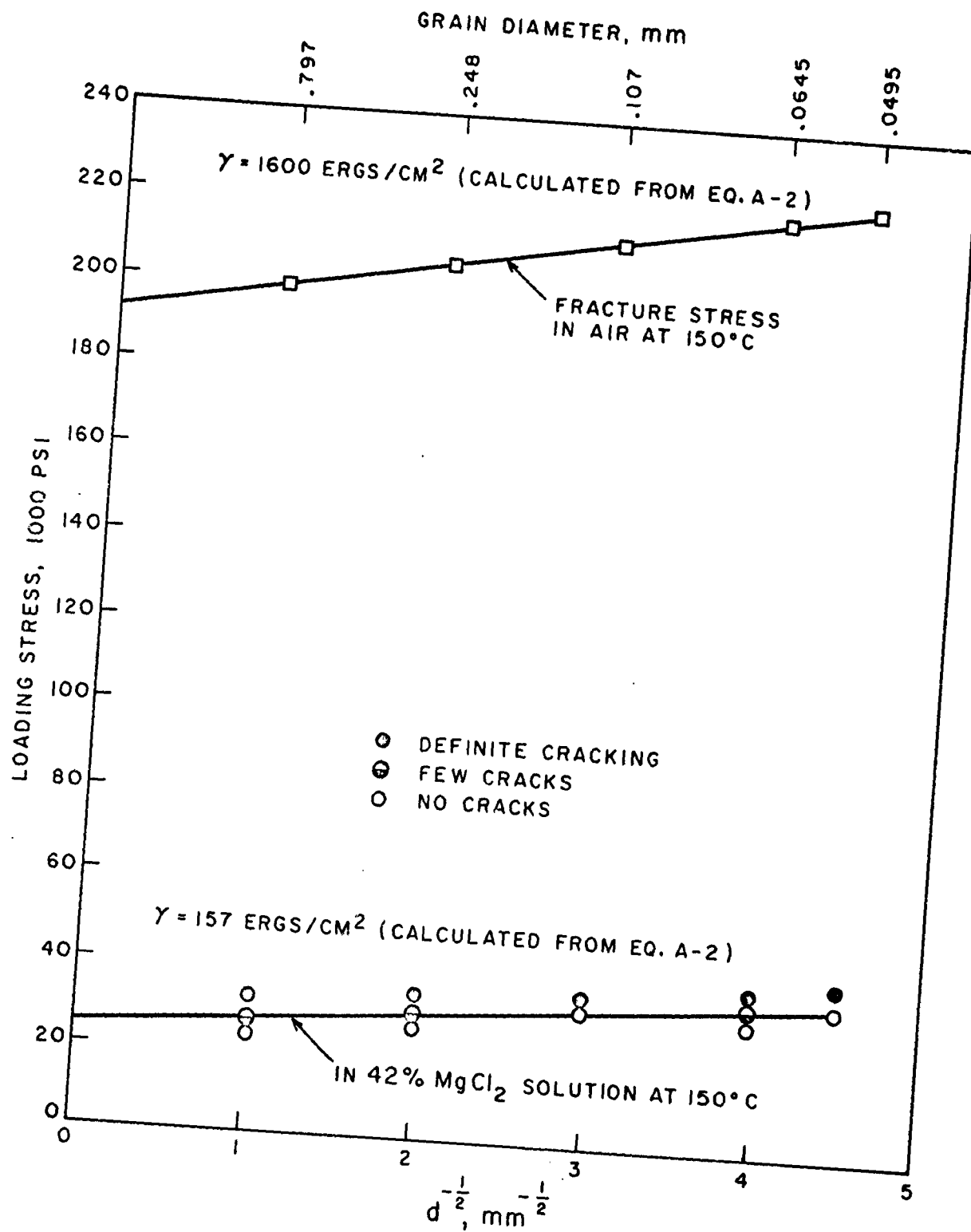| Material	Environment	Calculated Surface Energy, ergs/cm^2
304 Stainless Steel	Air at 150°C	1600
	$MgCl_2$ at 150° C	157
Mg-6% Al	Air at RT	1737
	$NaCl-K_2CrO_4$ at RT	93
Al-4% Cu	Air	ND[*]
	$NaCl-H_2O$ at RT	160
Armco Iron	Air	ND
	Boiling $Ca(NO_3)_2 \cdot 4H_2O-NH_4NO_3$	32

[*] ND - Not determined.
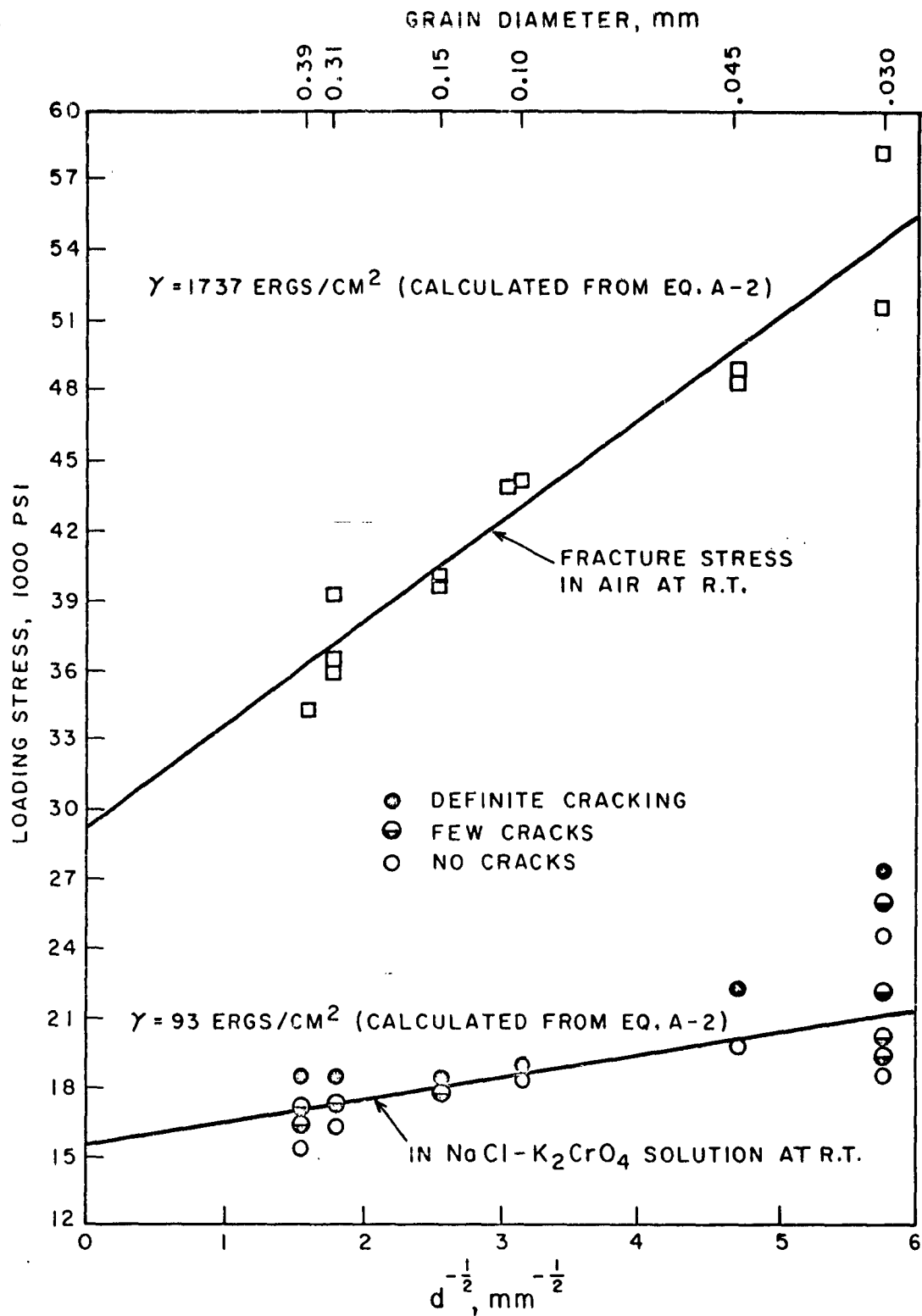
Figure A-1 - Stress Corrosion of Stainless Steel.

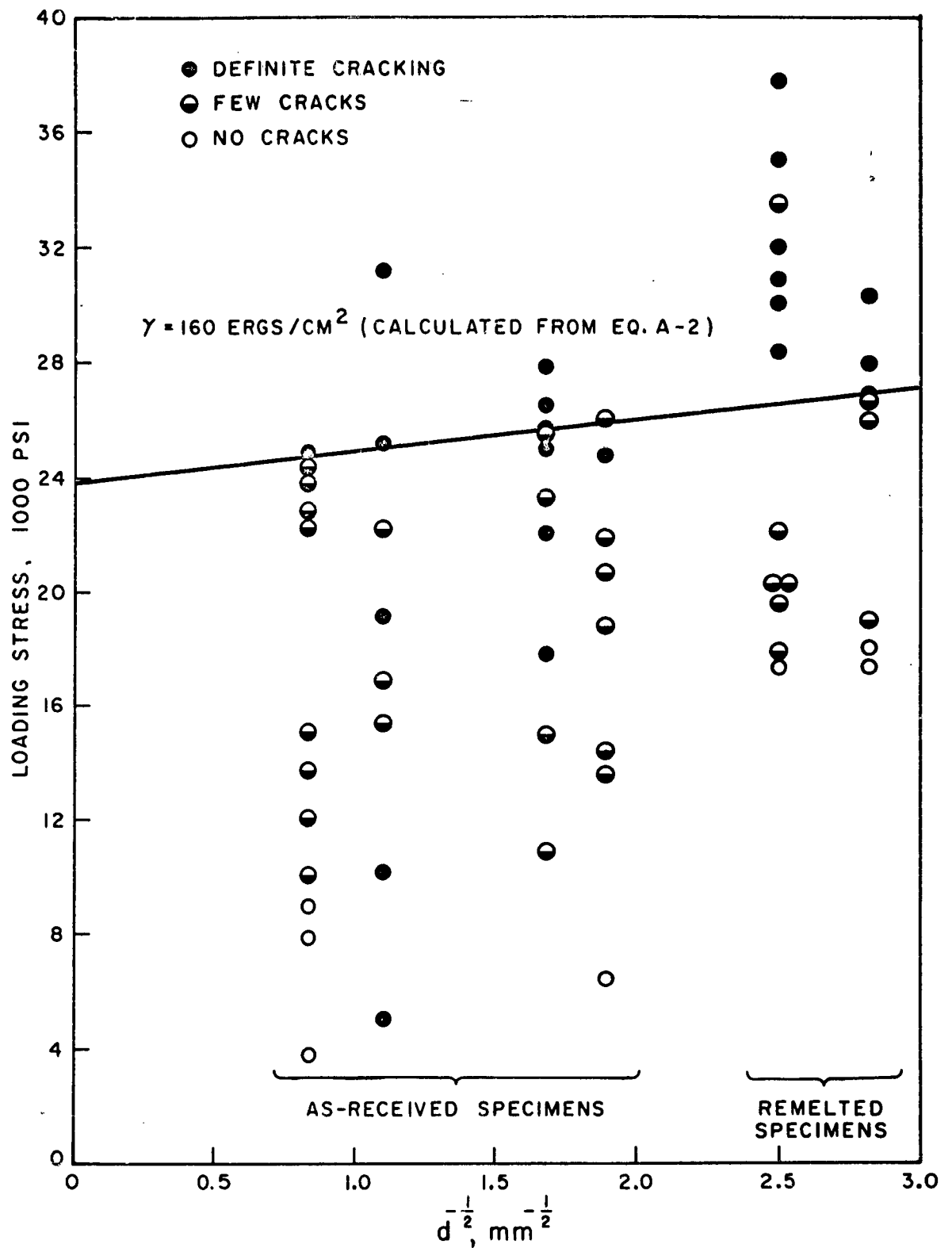Figure A-2 - Stress Corrosion of Mg-6Al.

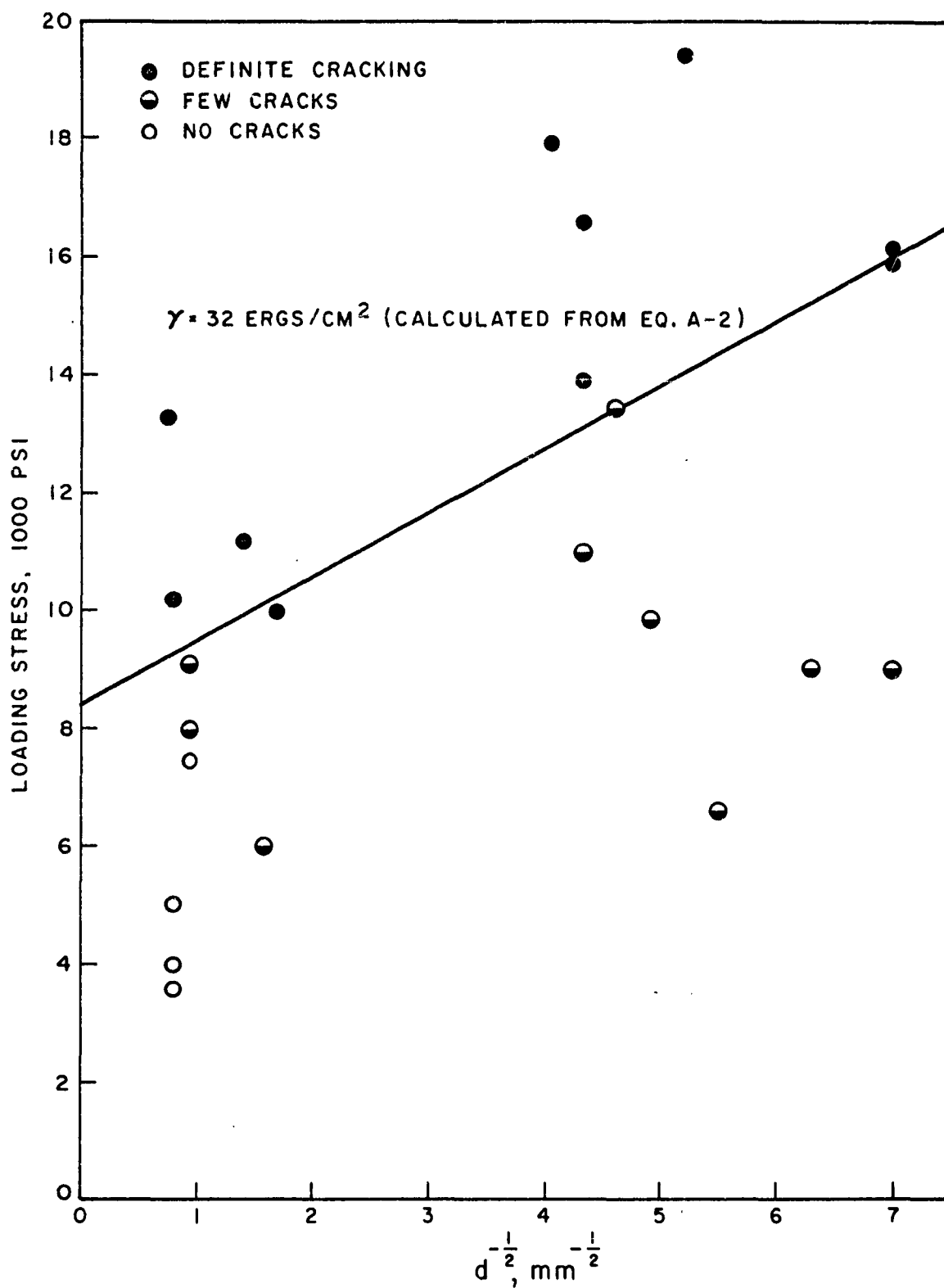Figure A-3 - Stress Corrosion Cracking of Al-4% Cu Alloy In
NaCl-H$_2$O$_2$ Solution.

Figure A-4 - Stress Corrosion Cracking of Armco Iron In
Boiling Ca(NO$_3$)$_2$ · 4H$_2$O - (NH4) NO$_3$ Solution.

ARF 2152-18

DISTRIBUTION LIST

Organization

Office of Naval Research
Department of the Navy
Building T-3
Washington 25, D. C.
Attn: Mr. Edward I. Salkovitz
      Head, Metallurgy Branch (2)

Commanding Officer
Office of Naval Research
Branch Office
86 E. Randolph Street
Chicago 1, Illinois (2)

Assistant Naval Attache for Research
Office of Naval Research
Branch Office, London
Navy 100, Box 39
F. P. O. , N. Y. , New York (5)

Director
U. S. Naval Research Laboratory
Washington 25, D. C.
Attn: Technical Information
      Officer, Code 2000 (6)
     : Code 2020   (1)
     : Code 6200   (1)
     : Code 6300   (2)
     : Code 6100   (1)

Chief, Bureau of Weapons
Department of the Navy
Washington 25, D. C.
Attn: RRMA   (1)
    : RREN-6 (1)

Commanding Officer
U. S. Naval Air Material Center
Philadelphia, Pennsylvania
Attn: Aeronautical Materials
      Laboratory   (1)

Superintendent
U. S. Naval Weapons Factory
Washington 25, D. C.
Attn: Code 720   (1)

Commanding Officer
U. S. Naval Ordnance Laboratory
White Oaks, Maryland   (1)

Commanding Officer
U. S. Naval Proving Ground
Dahlgren, Virginia
Attn: Laboratory Division   (1)

Chief, Bureau of Ships
Department of the Navy
Washington 25, D. C.
Attn: Code 330   (1)
    : Code 337L   (1)
    : Code 343   (1)

Commanding Officer
U. S. Naval Engineering Experiment
    Station
Annapolis, Maryland
Attn: Metals Laboratory   (1)

Materials Laboratory
New York Naval Shipyard
Brooklyn 1, New York
Attn: Code 907 (1)

Chief, Bureau of Yards and Docks
Department of the Navy
Washington 25, D. C.
Attn: Research & Standards Div. (1)

Commanding Officer
David Taylor Model Basin
Washington 7, D. C. (1)

Post Graduate School
U. S. Naval Academy
Monterey, California
Attn: Dept. of Metallurgy (1)

Office of Technical Services
Department of Commerce
Washington 25, D. C. (1)

Commanding Officer
U. S. Naval Ordnance Test Station
Inyokern, California (1)

Armed Services Technical
Information Agency (ASTIA)
Documents Service Center
Arlington Hall Station
Arlington, Va. (10)

Commanding Officer
Watertown Arsenal
Watertown, Massachusetts
Attn: Ordnance Materials
    Research Office   (1)
   : Laboratory Division   (1)

Commanding Officer
Office of Ordnance Research
Box CM, Duke Station
Duke University
Durham, North Carolina
Attn: Metallurgy Division   (1)

Commander
Wright Air Development Center
Wright-Patterson Air Force Base
Dayton, Ohio
Attn: Aeronautical Research
    Lab. (WCRRH)   (1)
   : Aeronautical Research
    Lab. (WCRRL)   (1)
   : Materials Laboratory
    (WCRTL)   (1)

U. S. Air Force ARDC
Office of Scientific Research
Washington 25, D. C.
Attn: Solid State Division
    (SRQB)   (1)

National Bureau of Standards
Washington 25, D. C.
Attn: Metallurgy Division   (1)
   : Mineral Products Div.   (1)

National Aeronautics Space
Administration
1512 H Street, N. W.
Washington 25, D. C.   (1)

National Aeronautics Space
Administration
Lewis Flight Propulsion Lab.
Cleveland, Ohio
Attn: Materials and Thermo-
       dynamics Division (1)

U. S. Atomic Energy Commission
Washington 25, D. C.
Attn: Technical Library (1)

U. S. Atomic Energy Commission
Washington 25, D. C.
Attn: Metals and Material Branch,
       Division of Research (1)
    : Eng. Develop. Branch,
       Div. of Reactor Develop. (1)

Argonne National Laboratory
P. O. Box 299
Lemont, Illinois
Attn: H. D. Young, Librarian (1)

Brookhaven National Laboratory
Technical Information Division
Upton, Long Island
New York
Attn: Research Library (1)

Union Carbide Nuclear Co.
Oak Ridge National Laboratory
P. O. Box P
Oak Ridge, Tennessee
Attn: Metallurgy Division   (1)
    : Solid State Physics Div. (1)
    : Laboratory Records
       Dept.   (1)

Los Alamos Scientific Lab.
P. O. Box 1663
Los Alamos, New Mexico
Attn: Report Librarian   (1)

Union Carbide Nuclear Co.
K-25 Plant Records Dept.
P. O. Box P
Oak Ridge, Tennessee   (1)

Union Carbide Nuclear Co.
Y-12 Plant Records Dept.
Central Files
P. O. Box Y
Oak Ridge, Tennessee   (1)

General Electric Company
P. O. Box 100
Richland, Washington
Attn: Technical Information
      Division   (1)

Iowa State College
P. O. Box 14A, Station A
Ames, Iowa
Attn: F. H. Spedding   (1)

ARMOUR RESEARCH FOUNDATION OF ILLINOIS INSTITUTE OF TECHNOLOGY

Knolls Atomic Power Laboratory
P.O. Box 1072
Schenectady, New York
Attn: Document Librarian (1)

Mound Laboratory
Monsanto Chemical Co.
P.O. Box 32
Miamisburg, Ohio (1)

U.S. Atomic Energy Commission
New York Operations Office
70 Columbus Avenue
New York 23, New York
Attn: Document Custodian (1)

Sandia Corporation
Sandia Base
Alburquerque, New Mexico
Attn: Library (1)

U.S. Atomic Energy Commission
Technical Information Service Extension
P.O. Box 62
Oak Ridge, Tennessee
Attn: Reference Branch (1)

University of California
Radiation Laboratory
Information Division
Room 128, Building 50
Berkeley, California
Attn: R. K. Wakerling (1)

Bettis Plant
U.S. Atomic Energy Commission
Bettis Field
P.O. Box 1468
Pittsburgh 30, Pennsylvania
Attn: Mrs. Virginia Sternberg,
    Librarian   (1)

Officer in Charge
U.S. Naval Civil Engineering
Research and Evaluation Lab.
Construction Battalion Center
Port Hueneme, California   (1)

Defense Metals Information Center
Battelle Memorial Institute
505 King Avenue
Columbus 1, Ohio   (2)

Solid State Devices Branch
Evans Signal Laboratory
U.S. Army Signal Engineering
Laboratories
c/o Senior Navy Liaison Officer
U.S. Navy Electronic Office
Fort Monmouth, New Jersey   (1)

Commanding Officer and Director
U.S. Naval Civil Engineering Lab.
Port Hueneme, California
Attn: Chemistry Division   (1)

Commanding Officer
U.S. Naval Ordnance Underwater
Station
Newport, Rhode Island   (1)

ARMOUR RESEARCH FOUNDATION OF ILLINOIS INSTITUTE OF TECHNOLOGY

ARF 2152-18
(Final Report)

U.S. Bureau of Mines
P.O. Drawer B
Boulder City, Nevada
Attn: Electro-metallurgical
    Division (1)

U.S. Bureau of Mines
Washington 25, D.C.
Attn: Dr. E. T. Hayes (1)

Commanding General
U.S. Army Ordnance
Frankford Arsenal
Philadelphia 37, Pa.
Attn: Mr. Harold Markus
    ORDBA-1320, 64-4 (1)

Prof. D. C. Grahame
Department of Chemistry
Amherst University
Amherst, Massachusetts (1)

Dr. J. E. Draley
Argonne National Laboratories
Box 299
Lemont, Illinois (1)

Prof. H. E. Farnsworth
Brown University
Providence 12, Rhode Island (1)

Prof. H. W. Paxton
Department of Metallurgical
Engineering
Carnegie Institute of Technology
Pittsburgh 13, Pennsylvania   (1)

Dr. W. R. Scott
Crest Research Laboratories Inc.
P.O. Box 8016
Seattle 55, Washington   (1)

Corrosion Research Division
Engineering Laboratories
E. I. DuPont de Nemours & Co.
Wilmington, Delaware   (1)

Dr. M. T. Simnad
General Atomics
P.O. Box 608
San Diego, California   (1)

Prof. M. Metzger
Department of Mining
And Metallurgy
University of Illinois
Urbana, Illinois   (1)

Mr. F. L. LaQue
International Nickel Company
67 Wall Street
New York, New York   (1)

Prof. H. H. Uhlig
Department of Metallurgy
Mass. Institute of Technology
Cambridge 39, Massachusetts (1)

Prof. M. E. Straumanis
School of Mines and Metallurgy
University of Missouri
Rolla, Missouri   (1)

ARF 2152-18
(Final Report)

Prof. M. G. Fontana
Department of Metallurgy
Ohio State University
Columbus, Ohio (1)

Prof. R. Speiser
Department of Metallurgy
Ohio State University
Columbus, Ohio (1)

Prof. J. O'M. Bockris
Department of Chemistry
University of Pennsylvania
Philadelphia, Pennsylvania (1)

Dr. A. Wachter
Corrosion Division
Shell Oil Development Co.
Emeryville, California (1)

Prof. N. Hackerman
Department of Chemistry
University of Texas
Austin, Texas (1)

Dr. Milton Stern
Union Carbide & Carbon Co.
Research Laboratories
Niagara Falls, New York (1)

Prof. A. T. Gwathmey
Dept. of Chemistry
University of Virginia
Charlottesville, Virginia (1)

Dr. E. A. Gulbransen
Westinghouse Electric Corp.
Research Laboratories
Beulah Road
Churchill Borough
Pittsburgh 35, Pennsylvania   (1)

Prof. W. D. Robertson
Dept. of Metallurgy
Yale University
New Haven, Connecticut   (1)

Reactor Development Board
Code 1500
Bureau of Ships
Department of the Navy
Washington 25, D. C.   (1)

Prof. P. Delahay
Department of Chemistry
Louisiana State University
Baton Rouge, Louisiana   (1)

Prof. P. Van Rysselberghe
Department of Chemistry
Stanford University
Palo Alto, California   (1)

Deterioration Prevention Center
2101 Constitution Avenue
Washington 25, D. C.   (1)

Dr. J. F. Eckel
Head, Dept. of Metallurgy
Engineering
Virginia Polytechnic Institute
Blacksburg, Virginia (1)

Mr. F. L. Whitney, Jr.
Corrosion Section
Research and Engineering Div.
Monsanto Chemical Company
St. Louis 4, Missouri (1)

Mr. H. Logan
Bureau of Standards
Div. 84 Rm 201a Bldg. NW
Washington 25, D. C. (1)

Prof. B. Chalmers
Department of Metallurgy
Harvard University
Cambridge, Massachusetts (1)

Prof. G. Hill
Department of Chemistry
University of Utah
Salt Lake City, Utah (1)

Dr. H. T. Francis
Armour Research Foundation
Metals Research Department
3350 S. Federal Street
Chicago 16, Illinois (1)